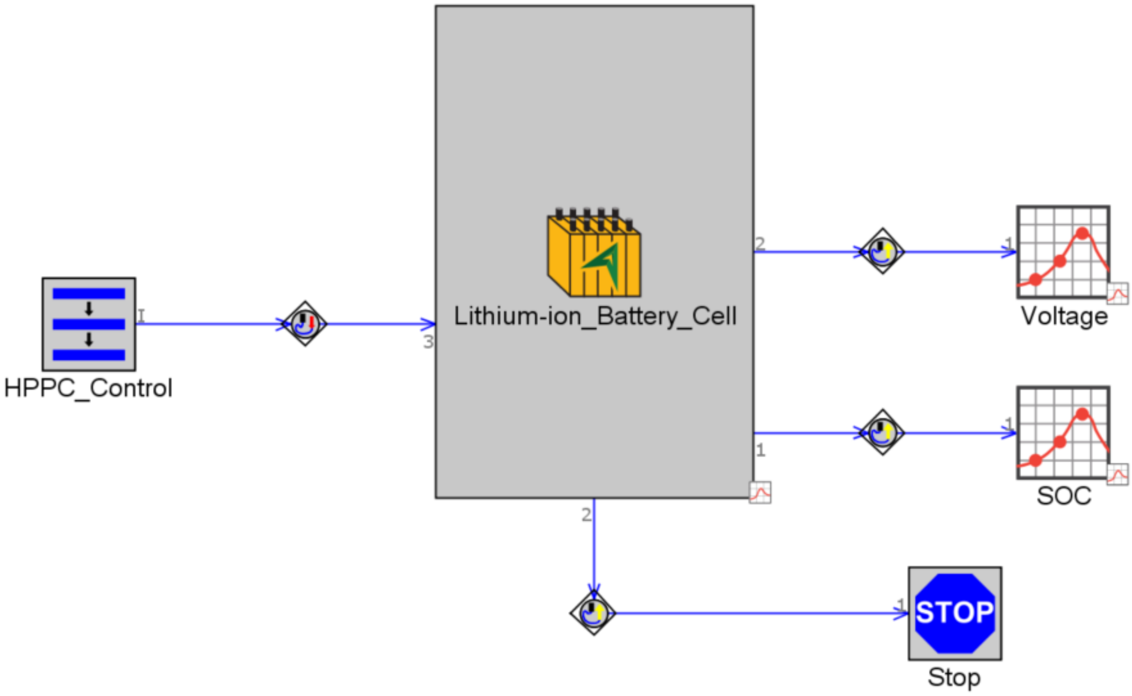

Chalmers University of Technology

Battery CAE Analysis

Master of Science Thesis

Anirudh Mehlawat
Mirza Ahsan Baig

Department of Electrical Engineering
CHALMERS UNIVERSITY OF TECHNOLOGY
Gothenburg, Sweden 2019

Master's thesis 2019

Validating dynamic behavior of Lithium ion battery cell

Validating dynamic behavior of battery cell with GT-Suite AutoLion and designing cell's surface temperature control system

Anirudh Mehlawat
Mirza Ahsan Baig

Department of Electrical Engineering
Division of Electric Power Engineering
Chalmers University of Technology
Gothenburg, Sweden 2019

Validating dynamic behavior of a Lithium ion battery cell

Validating the dynamic behavior of a battery cell with GT-Suite AutoLion and designing cell's surface temperature control system
Anirudh Mehlawat, Mirza Ahsan Baig

Supervisor: Björn Jonsson ,China Euro Vehicle Technology
Torbjörn Thringer, Chalmers University of Technology

Examiner: Torbjörn Thringer, Chalmers University of Technology

Master's Thesis 2019:
Department of Electrical Engineering
Division of Electric Power Engineering
Chalmers University of Technology
SE-412 96 Gothenburg
Telephone +46 31 772 1000

Cover: HPPC charging model of the battery cell in GTSuite AutoLion

Typeset in LaTeX
Printed by Chalmers Reproservice
Gothenburg, Sweden 2019

Validating the dynamic behavior of lithium ion battery cell
Validating the dynamic behavior of a battery cell with GT-Suite AutoLion and designing cell's surface temperature control system
Anirudh Mehlawat and Mirza Ahsan Baig
Department of Electrical Engineering
Chalmers University of Technology

Abstract

In this thesis, the dynamic behavior of a lithium ion cell was investigated using a hybrid pulse power characterization (HPPC) test under different temperatures with different charging-discharging rates. Secondly, a water-cooled and cell temperature control system was developed for a battery cell.

Considering the importance of having a good prediction of the generated heat during the charging-discharging process, a water-cooling system for a battery cell was designed and controlled by a developed PID algorithm considering the surface temperature of the battery cell and a water flow in the cooling plates. The DC pump, driving the water flow through the cooling plates was controlled by an Arduino micro controller, in which a Python program was installed. Initially the battery is charged-discharged without any cooling setup and the maximum temperature rise is observed. After that, with the cooling system, a reduction in battery surface temperature was observed, when the battery cell surface temperature is controlled to the specific temperature of 27°C, which can provide a prolonged life to the battery cell. Further the power loss was validated by measuring it to $1.90W$ using the calorimetry method, very close to the calculated value of $2.0W$.

To predict the dynamic behavior of a Lithium-ion battery cell, an electro-thermal model can be represented by an R_0+2RC equivalent circuit. The goal is to estimate the parameters, as well as the relation between open circuit voltage(OCV) and the state of charges(SoC) through a hybrid pulse power characterization(HPPC) test under different temperatures. The obtained results were validated with GT-Suite Auto-Lion, by estimating and comparing the $R_0 + 2RC$ parameters, finally optimized the HPPC - OCV Auto-Lion results with respect to the experimental test results, an accuracy of the physical battery cell replica in GT-Suite-Auto-Lion, the error between the two HPPC- OCV results was reduced by 1% from 3% to 2%.

Keywords: Lithium ion battery, Hybrid Pulse Power Characterization test (HPPC), GT-Suite, AutoLion, PID Algorithm, Battery Cooling System, EVs and HEVs.

Acknowledgements

This thesis work has been carried out at the Division of Electric Power Engineering, Department of Electrical Engineering at Chalmers University of Technology, Gothenburg, Sweden and CAE Energy Department at China Euro Vehicle Technology, Gothenburg, Sweden.

We would like to express our thanks to the following people,

- Our supervisor and examiner Prof. Torbjörn Thiringer at Chalmers University of Technology for supporting us with the project and giving valuable feedback on our work. And, Chengjun Tang for helping us during the project work.
- Our supervisor Björn Jonsson and Christèle Grimaud at China Euro Vehicle Technology(CEVT) for providing us an opportunity to work along with them.
- And, would like to specially thank Joe Wimmer and his team from Gamma Technologies for all the help with GT-Suite AutoLion.

Anirudh and Ahsan, Gothenburg, 2019.

Contents

List of Abbreviation

Variables for Governing Equations

- x - Distance in the through-plane direction
- σ_s - Solid phase conductivity
- ϕ_s - Solid phase potential
- ϕ_e - liquid phase potential
- α_{dl} - Specific interfacial area
- C - Specific capacitance
- j^{Li} - Reaction current of Li
- κ^{eff} - Electrolyte effective ionic conductivity
- κ_D^{eff} - Effective diffusional conductivity
- c_e - Li^+ concentration in the electrolyte
- C_s - Li^+ concentration in solid
- ϵ - Porosity
- D_e^{eff} - Electrolyte phase Li diffusion coefficient
- t_+^0 - Transference number
- F - Faraday's constant
- r - Particle radius

Others used in this work

- EVs - Electric Vehicles
- HEVs - Hybrid Electric Vehicles
- Li-ion - Lithium Ion
- PWM - Pulse Width Modulation
- GHGs - Green house gasses
- PID - Proportional Integral Derivative
- OCV - Open Circuit Voltage
- HPPC - Hybrid pulse power characterization
- SoC - State of Charge
- LIBs - Lithium ion batteries
- ECM - Equivalent Circuit Model
- P2D - Pseudo-2 dimension
- C-Rate - Current Rate

List of Figures

List of Tables

1 Introduction

1.1 Background

The Paris agreement, due to which several regulations came into operating to work on climate changes which emphasize on regulation for the automotive industry and one of the strict regulations to reduce emissions of green house gases (GHG) from automobiles, supported the rise of Hybrid Electric Vehicles as well as Electric Vehicles. The new developments in the automotive industry gave rise to new variants of power trains to develop, where the batteries play the role of energy source for the vehicle. Among various chemistry of batteries, Lithium-ion batteries(LIBs) are preferred for EVs and HEVs due to their high energy efficiency and high power density, in comparison with other batteries [4]. Lithium ion batteries are electrochemically and thermally stable, have long battery life, low self-discharge rate, a potential to charge or discharge rapidly and less maintenance [5].

Although LIBs have been playing a significant role in the automotive industry for almost a decade, there are still a lot of areas of research for LIBs which can help in improving the efficiency and performance of the battery pack for EVs and HEVs. One of the challenges in improving lithium-ion batteries is to determine its behavior under various operating conditions. To evaluate their behavior, Li-ion batteries can be represented by empirical models and electrochemical models. Empirical model, such as equivalent circuit models(ECM) are used to represent batteries in various applications such as in power systems or automotive industries[6],[7],[8]. The elements of these models are estimated by charge or discharge of a battery and investigating the current/voltage response. Although these models are simple and computationally fast to predict the battery behavior but they are not capable to estimate the battery's physics based parameters. On the other hand, electrochemical models are based on electrochemical reactions and physics based governing equations. The Psuedo-2D model is one of the popular electrochemical model. It has been used in battery investigations to predict the behavior of Li-ion batteries.

Besides understanding the Li-ion battery cell behavior under various conditions, reduction of its power or heat losses is also an aspect to improve the battery cell's life.

1.2 Aim

The first aim of this thesis is to model a battery cell in GT-Suite AutoLion which can validate the dynamic behavior of a physical cell by performing a Hybrid Pulse Power Characterization (HPPC) and validate the parameters estimated from experimental results, secondly, to develop a cooling mechanism for the battery cell which will be controlled by implementing a control algorithm, controlling the cell surface temperature by adjusting the water flow rate.

1.3 Scope

1.3.1 Calorimetry – Lithium Ion cell cooling setup

For the battery test setup, a cooling system was designed to cool a battery cell temperature controlling the flow rate of water. A control mechanism was developed to maintain the surface temperature of the battery cell at a fixed value by using a control algorithm. In the cooling system, when the surface temperature of the cell is higher than the reference value, the developed control algorithm shall keep it closer to the reference temperature. The cell is to be kept in a Styrofoam box to test the setup, two different types of sensors were calibrated and the thermal resistance between cell and surrounding of the Styrofoam box will be estimated and validated.

1.3.2 Battery cell dynamic behavior study

With an aim to study the dynamic behavior of the physical battery cell, a hybrid pulse power characterization test performed at different temperatures with different current rates (C-Rate). The test was performed with an intention to investigate the variation in internal impedance of the battery cell at different state of charges (SoC) and temperatures. The parameters for the equivalent circuit model (ECM) are estimated using a nonlinear least-square curve fitting method to study the variation in internal impedance of the battery cell. The bench age of the cell is unknown, and the effect of the battery cells' calendar aging is not considered in order to extract the parameters at two different temperatures.

1.3.3 Model Validation for dynamic behavior

The dynamic behavior of the battery cell will be validated by using an electrochemical model in GT-Suite-AutoLion. A LIB will be modeled in GT-Suite-AutoLion and various other models such as, HPPC test model, OCV optimization model, HPPC voltage validation model, will also produce results which will be validated by the measurements obtained from experimental results using the similar conditions and parameters. Due to the unavailability of data for the battery cell aging for this cell, degradation is not considered while validating the parameters of the electrochemical model. Besides the cell degradation, other parameters such as ionic conductivity, ionic diffusivity, entropic heat generation and exchange current density of the electrodes are not considered while designing the electrochemical model. All these parameters do affect the output to a considerable amount.

1.4 Sustainable Environment and Ethical Aspects

The battery degradation and its performance are issues related to EVs and HEVs, so getting familiar with the dynamic behavior of the battery will help in understanding the influence of the various parameters on the battery's performance. Therefore, an electro-thermal model was used to study the battery's operation also including its thermal behaviour. Due to the lengthy lifetime of batteries, a reduction in the number of damaged batteries as well as in their environmental impact can be observed, consequently, it will motivate more people to move towards EVs and HEVs and subsequently, there is a potential for a reduction of emission of GHGs. The designed cooling control mechanism, as well as other efficient cooling systems, will also help in increasing the lifetime of the battery by protecting them from overheating, voltage losses, capacity losses and electro-chemistry losses which can affect the battery life after 500-800 cycles and such control systems contribute towards making these batteries to perform efficiently by reducing the power losses or regulating the generated heat which can not affect the electro-chemistry of the battery cell to protect the drop in capacity and hence to save the operating voltage of the battery cell in longer duration's.

2

Theory

2.1 Lithium-ion Battery Cell

In this section, the basic description of the battery cell is given along with the necessary parameters required to build an electrochemical model battery cell in GT-Suite-AutoLion. The battery cell is represented by ECMs, secondly, the comparison between different ECMs, description of the thermal equivalent model of the battery cell was explained and lastly, the electrochemical model was explained briefly with parameters required to build an optimization model for the battery cell.

2.1.1 Description of battery cell

The battery cell shown in fig 2.1 was used in this thesis. It's a commercial $26Ah$ lithium-ion pouch cell. Based on the manufacturer data its voltage range is $2.8V$ to $4.15V$, corresponding to 0 to 100% SOC level respectively. The positive electrode consists of a mixture of lithium manganese oxide (LMO) and lithium nickel cobalt manganese oxide (NMC) and the material for the positive tap is aluminum whereas the negative electrode consists of natural graphite and the corresponding tap material is nickel-plated copper. The data set about the cell configuration and parameters used are briefly explained [9] in the work.

Figure 2.1: Lithium-ion battery cell

2.1.2 Parameters used for Electro-chemical model

Various parameters are required to build a physics based model representing the battery cell, which are taken from literature [9]. The battery cell basic description table 2.1 parameters, similarly parameters used in electrochemical model cell in table 2.2 and 2.3. All the collected parameters are presented from literature work [9].

Table 2.1: Lithium-ion Battery cell Description

Parameters	Description
Battery cell type	Prismatic type(soft pack):Al foil pouch
Nominal Capacity	26 Ah
Voltage range (continuous)	2.8-4.15 (V)
Length(mm)	232
Width (mm)	165 (folded), 171 (not folded)
Thickness(mm)	7.65

Table 2.2: Parameters used in electrochemical model

Parameters	Cathode	Anode
Material Thickness, L_s(μm)	74	64.5
Foil Thickness, L_{cc}(μm)	20	10
Conductivity, (Σ_s)(S/m)	100	100
Diffusivity, ($Ds(m^2/s)$)	$E^{-}14$	$1E^{-}13$
Bruggeman constant electrodes, (β_s)	1.5	1.5
Bruggeman constant electrolyte, (β_l)	3	2.5
Anode to cathode transfer coefficient($\alpha_{a/c}$)	0.5	0.5

Table 2.3: Electrolyte parameters used in electrochemical model

Parameters	Value
Double layer capacitance, $C_{dl}(F/m^2\text{m})$	0.2
Separator Thickness, L_{sep}(μm)	16
Electrolyte Concentration,(mol/m^3)	1000
Diffusivity, $D_l(m^2/s)$	$3E^{-}10$
Electrolyte conductivity,$K_l(S/m)$	0.005

2.2 Battery Equivalent Electrical Circuit

The ECM has several models ranging from 0RC, 1RC, 2RC to 6RC and more branches. Additional branches increase the complexity in the calculations although it provides more accurate results than the former. All models consist of various electrical elements to represent a battery and for this thesis, only a $R0 + 2RC$ ECM model is considered.

2.2.1 Equivalent Electrical Circuit models

The performance of a cell at different conditions can be estimated through simulation of ECM as indicated by [10]. ECMs are widely used to represent the battery dynamic behavior by evaluating SOC levels and predicting battery performance in a battery management system [10]

The equivalent circuit model for a 0-RC Model represents the circuit consisting an internal resistance R_0, an ideal voltage source(OCV) as a function of SOC, i_b is the battery output current, which is termed as positive for discharging and negative for charging and V_b is the battery terminal voltage as shown in fig 2.2, but this model does not represent the transient behavior of a lithium-ion battery cell, although it is easier to compute the parameter but it is not acceptable for the dynamical representation of the battery cell[5].

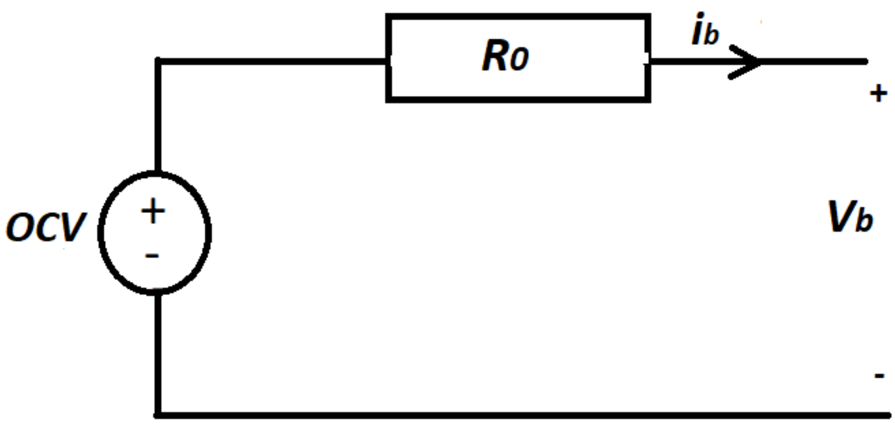

Figure 2.2: R_0 Internal resistance circuit model

The second model is defined as a single time constant (STC) model, and a parallel RC network is added in series with the internal resistance R_0 of the previous model, to approximate the dynamic behavior of the battery cell, which is shown in fig 2.3. The added parameters are R_1 and C_1, to produce the transient response while charging or discharging the battery cell or relaxing [10].

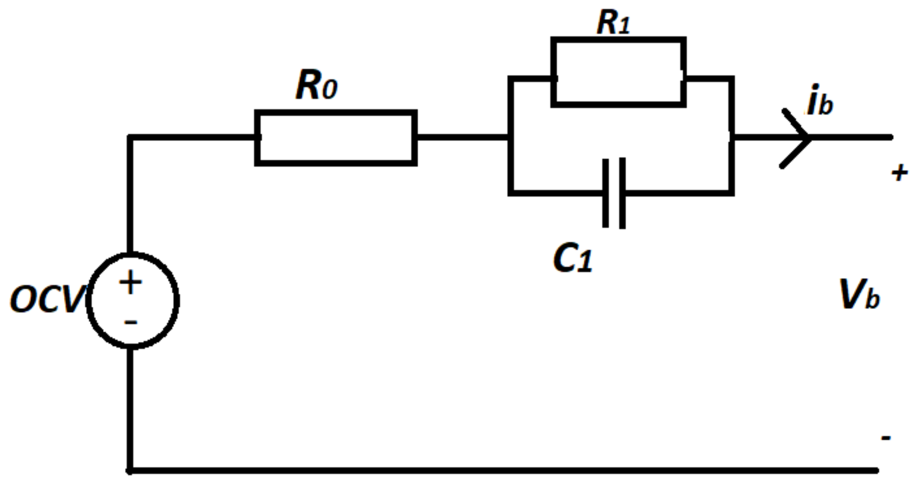

Figure 2.3: $R_0 + R_1C_1$ (STC) circuit model

A double time constant (DTC) model consists of an internal resistance, R_0, two RC branches (R_1,C_1) and (R_2,C_2), an ideal voltage source (OCV) and a terminal battery voltage, V_b. A DTC model have two different time constants, a slow time constant ($\tau_1 = R_1C_1$) and a faster time constant($\tau_2 = R_2C_2$) representing approximate the transient dynamic behavior of the battery cell, as shown in fig 2.4. The DTC model represents a accurate transient behavior of the battery cell than the STC model, and these two time constants play a dominant role in the parameters identifications [10].

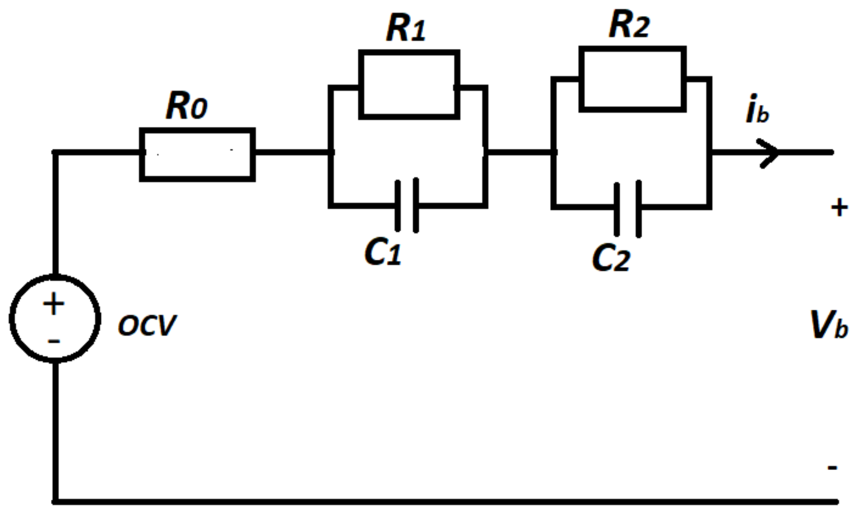

Figure 2.4: $R_0 + 2RC$ (DTC) circuit model

It is the preferred model since it describes the changes in the battery's dynamic behavior which occur due to mass transport effects and double layer effects as described by [10].

2.3 Thermal Equivalent model of the battery cell

The battery cell is represented by an electro-thermal model as shown in fig 2.5 consisting of two parts, an electrical model and a thermal model where heat generation from the battery cell and surface temperature of the cell are the factors considered to design the model[11]. It is a closed loop model, where surface temperature fed back to electrical model to calculate heat generation, as generated heat will affect the temperature of the battery cell.

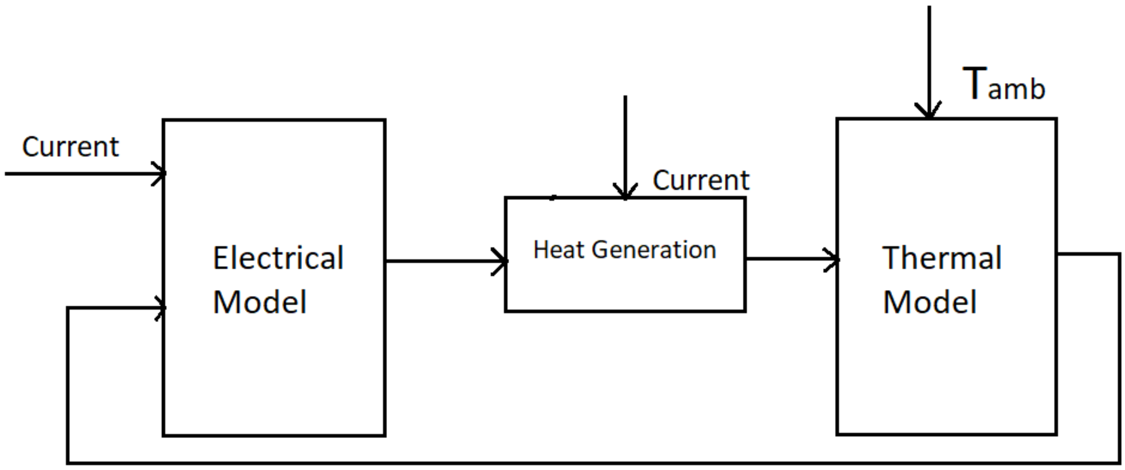

Figure 2.5: Electro-Thermal Model

The internal heat generation whilst performing the charging-discharging of the battery cell is based on work described by [12]. The generated heat equation can be expressed as the sum of reversible heat and irreversible heat or Joule heat and entropy heat, presented by 2.1 and 2.2.

$$q_t = q_j + q_e \tag{2.1}$$

$$q_t = I^2 R + IT \frac{\partial(U)}{\partial(t)} \tag{2.2}$$

In (2.1), $q_j(W)$ represents Joule heat as the irreversible heat, $q_e(W)$ is entropy heat which is the reversible heat, (I) is the current in the battery cell, (R) is the total resistance of the battery cell including resistance of the connecting wires, connected components as well, (T) is the temperature of the battery cell and $\partial(U)/\partial(t)$ is the entropy coefficient. Irreversible heat is the heat generated by the battery cell while charging-discharging which is accounted as power loss and reversible heat i.e, entropy of the battery cell is not discussed in thesis work as it is dependent on the total impedance of the battery cell while maintaining a constant temperature. However, entropy does influence the OCV as well as internal impedance of the battery cell significantly[13].

2.3.1 Thermal Model

The change in surface temperature of the battery cell used in the physical test setup is presented by the thermal equivalent model in fig 2.5 [13]. The thermal equivalent model consists of heat generated inside the cell represented by $q_t(W)$, a thermal heat capacity represented by $C_{th}(J/°\text{C})$, a thermal resistance $R_{th}(°\text{C}/W)$, a convective resistance $R_{conv}(°\text{C}/W)$, $T_s(°\text{C}/W)$, $T_{amb}(°\text{C}/W)$ is the ambient temperature. The thermal resistance measures the temperature difference between the surface temperature of the cell, the convective resistance is the temperature difference between the surface of the battery cell and the ambient. C_{th}, heat capacity indicates the dynamics of the temperature of the battery cell [11].

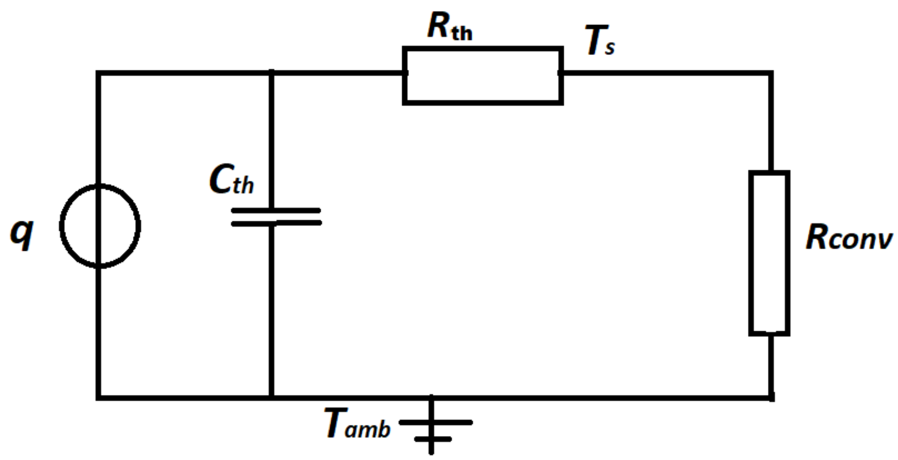

Figure 2.6: Thermal equivalent model of the battery cell

(2.3) governs the dynamics of the surface temperature T_s of the battery cell considering the ambient temperature T_{amb}, $R_{conv}(°\text{C}/W)$ was calculated according to (2.4) and the remaining parameters R_{th}, C_{th} were calculated by using non-linear curve fitting method in chapter 4.

T_s is found as

$$T_s(t) = T_{amb} + R_{conv}q(1 - \exp\frac{-t}{C_{th}(R_{th} + R_{conv}})) \tag{2.3}$$

where, R_{conv} was calculated by the relation

$$R_{conv} = \frac{T_{amb} - T_s}{q} \tag{2.4}$$

The surface temperature of the battery cell T_s was initially at ambient temperature T_{amb}, then it reached a steady state temperature of the cell, which makes it easier to calculate R_{conv} [11]. Fig 2.7, shows the exponential change in the temperature of the battery cell, when the battery cell generates heat while performing the discharging-charging. The surface temperature of the cell start from the ambient temperature and reaches to steady state temperature over a long period of time. Equation (2.3) provides the relation of the transient response of the battery cell temperature, which shows that the difference between initial and final temperature of the battery cell is controlled by a thermal resistance, R_{th} but the transient response was calculated by a thermal resistance R_{th} and thermal capacity, C_{th}.

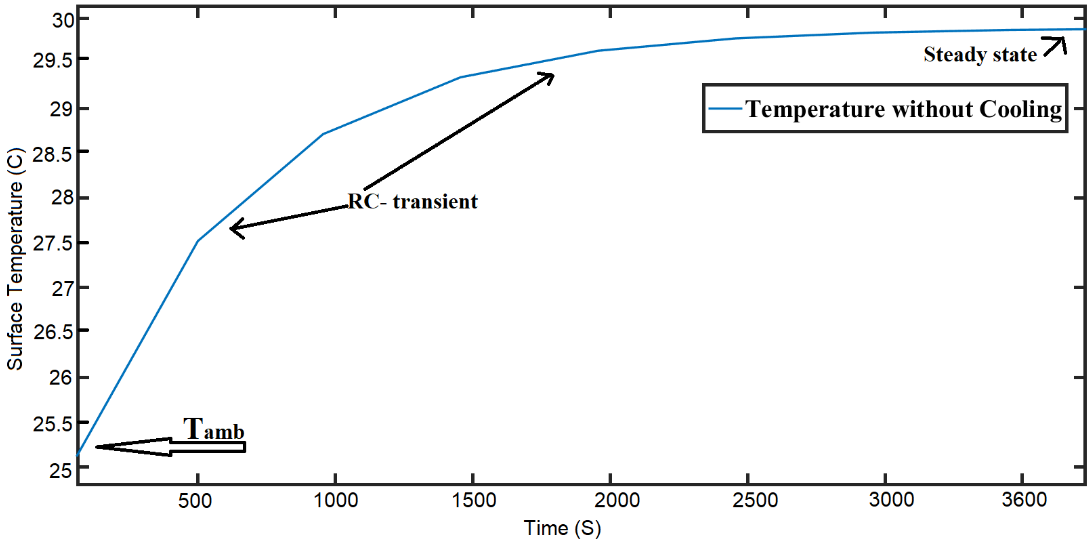

Figure 2.7: Transient temperature of the battery cell

2.3.2 Thermodynamics Law for calorimetry method

The thermodynamics's second law is used to calculate the power loss and the specific heat of the battery cell using the calorimetry method. A law which states that entropy of a closed system increases, which means that heat produced by the battery cell while discharging will transfer to the water flowing in the cooling plates [10], which is presented by 2.5, where Q_{loss} is the heat generated by the battery cell and Q_{water} is the heat absorbed by the water flowing in the cooling plates.

$$Q_{loss} = Q_{water} \tag{2.5}$$

Following the law of energy conservation presented by 2.5, the flow rate required to mitigate the generated heat was calculated, by using the expression 2.6.

$$Q_{loss} = \rho V C_w \Delta T_w \tag{2.6}$$

where, ρ is the water density, C_w is the specific heat capacity of the water, ΔT_w is the inlet and outlet temperature difference of water in the cooling plates and V

is the required flow rate. The required flow rate for the generated heat or power loss was measured by the linear relation shown in fig 4.2. The specific heat capacity of the battery cell was calculated by considering the change in the battery cell's temperature (ΔT_b), generated heat or power loss (Q) and the mass of the battery cell (M_b), as explained in the previous work [11].

$$Q = M_b C \Delta T_b \tag{2.7}$$

2.4 Electro-chemical Model

An electrochemical battery model was built in GT-Suite-AutoLion based on the John Newman model, which is defined as a Pseudo 2D (P2D) model. This model works by representing the Li^+ intercalation/de-intercalation reactions taking place inside the lithium-ion battery cell and predicts the voltage, current, power, heat generation, heat rejection. Fig 2.8, illustrates the basic terminology of the battery cell, presenting the transfer of lithium ions.

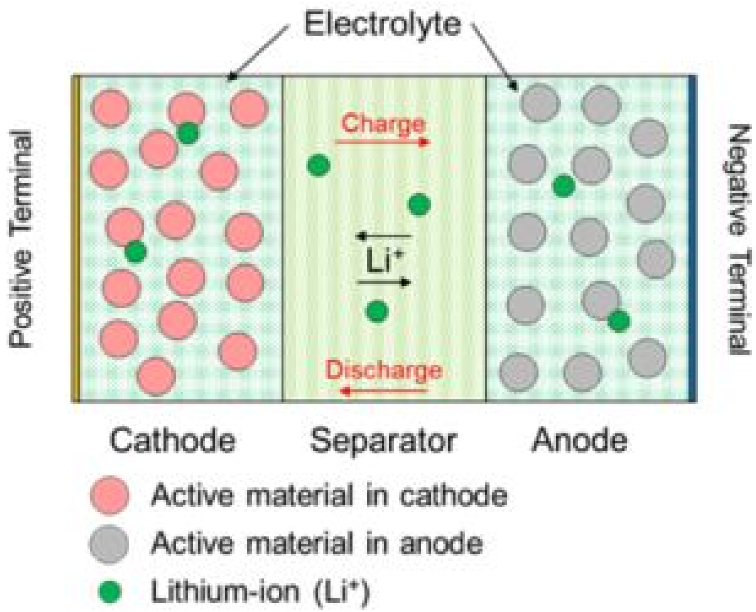

Figure 2.8: Schematic diagram of electrochemical model

when applying the current in either direction, redox(reduction-oxidation) reactions take place in the anode and cathode. During these reactions, Lithium ions (Li^+) and electrons (e^-) are captured and released. For this P2D model, the governing equations were implemented using the finite control volume approach. In each finite control volume of the cathode and separator, there is a representation of active material, each of which are discretized in a specified volume in the radial direction [14], [15].

The electrochemical reaction rate depends on an interfacial area of the particles of the electrode and the interaction between the electrodes and the electrolyte solution, which emphasizes on the porous theory of electrodes. Newman and Tiedeman, came up with a porous electrode theory for different battery applications. The electrodes are defined as porous blocks containing spherical particles surrounded by electrolyte as shown in fig 2.8. To understand the electrochemical model cell and its associated chemistry, few parameters of the governing equations were estimated using average quantities and continuous variables [7], resulting in introducing the Psuedo-2D model(P2D) model for batteries. The governing equations given in the table 2.1 describe various conditions as explained by [14], which describes the working methodology of an electrochemcial model cell.

	Description	Equation	Discretization
Charge Conservation	Solid - phase	$0=\partial\frac{}{\partial x(\sigma_s^{eff}\frac{\partial\phi_s}{\partial x})-j^{Li}-\alpha_{dl}C\frac{\partial(\phi_s-\phi_e)}{x}}$	Thru - Plane (Anode to cathode collector) direction
	Electrolyte-Phase	$0 = \partial(k^{eff}\frac{\partial\phi_e}{\partial x})\frac{}{\partial x+\frac{\partial(k_D^{eff}\frac{\partial \ln c_e}{\partial x})}{\partial x}+j^{Li}+a_{dl}C\frac{\partial(\phi_s-\phi_e)}{\partial x}}$	Thru - Plane (Anode to cathode collector) direction
Conservation	Electrolyte-Phase Li^+	$\partial\left[\epsilon c_e\right]\frac{}{\partial t=\frac{\partial}{\partial x}\left(D_e^{eff}\frac{\partial c_e}{}\right)+\frac{1-t_+^0}{F}j^{Li}}$	Thru - Plane (Anode to cathode collector) direction
	Active Material Li	$\partial C_s\frac{}{\partial t=\frac{1}{r^2}\frac{\partial}{\partial r}\left(D_s r^2\frac{\partial c_s}{\partial r}\right)}$	Radial direction

2.4.1 Parameters

Based on these governing equations, few parameters were chosen to estimate and to emulate the model battery cell. These parameters helped in balancing the electrochemical model cell and also helped in improving its performance.

2.4.1.1 N/P Ratio

The thickness of the electrodes in the electrochemical model are mentioned in battery cell description table 2.2. The N/P ratio was chosen as a parameters as it affects the cell's performance by identifying and developing a lithium plating while charging the battery cell [16]. Lithium plating results in reducing the capacity, mechanical swelling and potential internal short circuit, along with increasing internal resistance of the cell and affecting the porosity of the electrode [16], [17]. The N/P ratio's initial value was selected by observing the effect of the different N/P ratio values while discharging the model cell. Therefore, a cell discharging model was designed in GT-Suite-AutoLion and multiple discharge cycles were performed to observe the respective change in discharge results with the change in N/P ratio. While discharging the electrochemical model cell at 1C-Rate, there was no significant change in the results, hence, a slower rate, 0.2C-rate was opted to discharge the model battery cell and it does affect the cell's performance by reducing the usable capacity of the model cell, as it can be seen in fig 2.9.

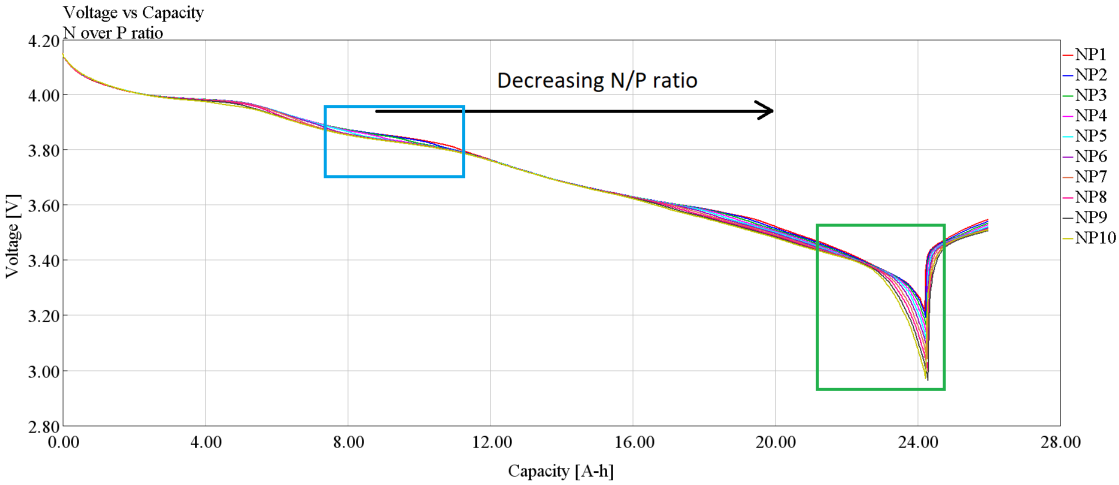

Figure 2.9: Discharging cycles of electrochemical model cell

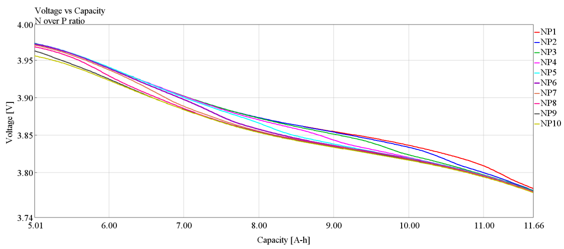

Figure 2.10: Blue Box

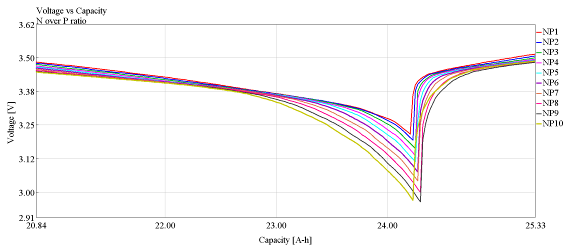

Figure 2.11: Green box

The enhanced picture of the blue box is shown in fig 2.10 representing the dip in operation potential range of the electrochemical model cell, similarly, the green box is shown in fig 2.11 representing the reduced capacity of the electrochemical model cell achieved while discharging the modeled cell with 0.2C rate. This attribute was varied from 1 to 1.45 in increments of 0.05 steps and with the increasing N/P ratio, the capacity of the electrochemical modeled cell decreased as well as the dip in operational potential was observed and the initial value chosen to be used in calibrating the cell was $NP7$, 1.35.

2.4.2 Contact Resistance

Contact resistance at the interface of electrodes and current collector in the electrode in a battery cell is a parameter which does affect the performance of the battery cell. Due to an irregular surface, surface imperfections and roughness, the transport of current occurs at only a few spots which are created by mechanical contacts [18], as shown in fig 2.12. The irregularity in between the surfaces will probably increase the internal resistance of the electrode, therefore reduces the usable capacity of the battery cell.

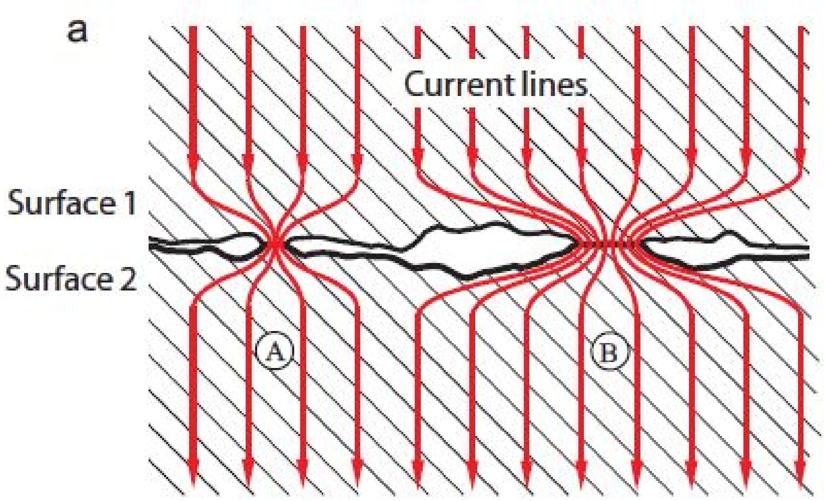

Figure 2.12: Conduction current paths in the contact interface of rough surfaces [1]

This attributes to the difference in the ohmic resistance of the battery cell including resistivity of electrodes and contact resistance. This attribute was varied from $0.001\Omega m^2$ to $0.002\Omega m^2$ in increments of 0.0002, and these variants do affect the performance of the model cell, which was observed by discharging the model cell with multiple cycles, where the varied results could be observed with a $1C$ rate and the chosen contact resistance was $CR5$ which is $0.0018\Omega m^2$. The results are presented in fig 2.13 showing the discharging profile of the model cell and further results showing the performance of the battery cell with individual contact resistance values, presented in fig 2.14.

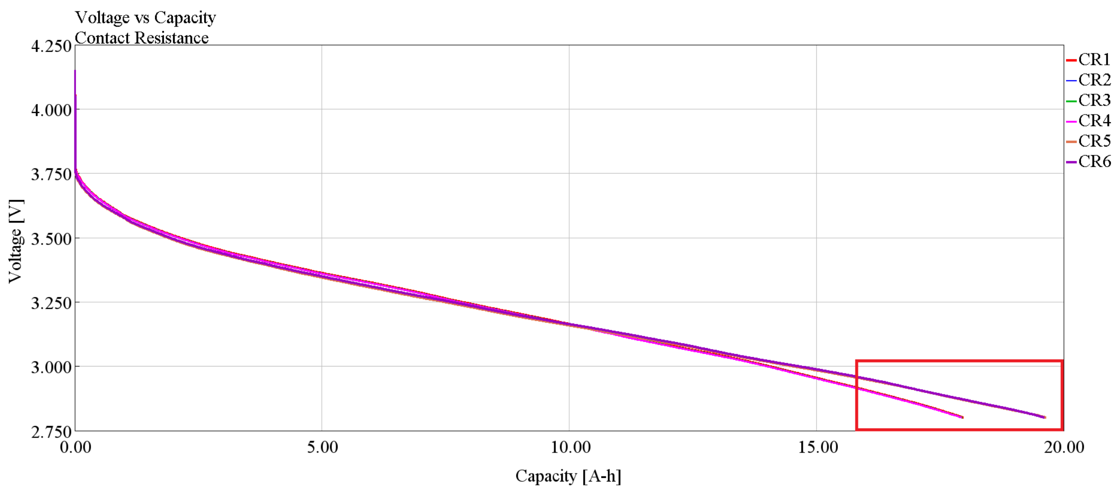

Figure 2.13: Change in capacity due to change in contact resistance

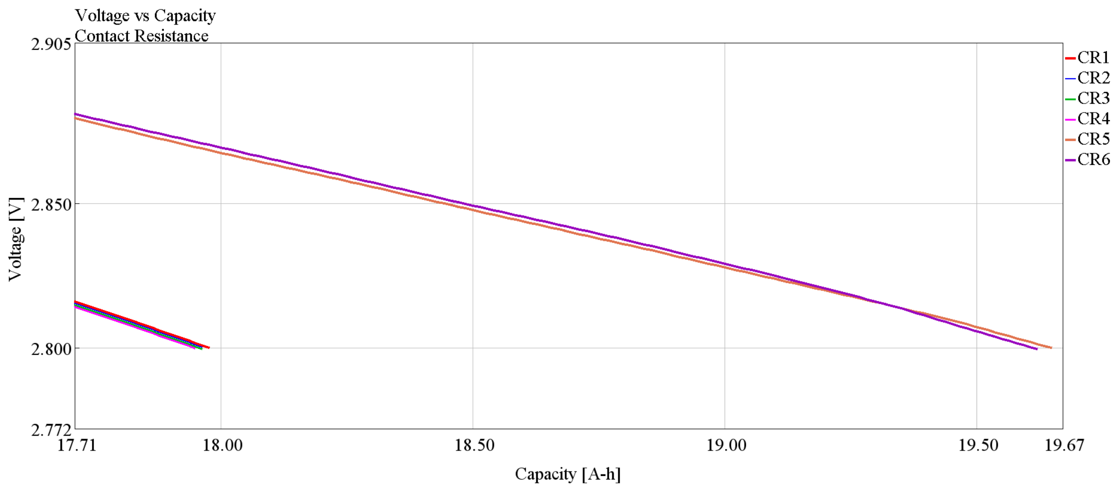

Figure 2.14: Zoom in - Red Box

2.4.3 Particle Size

The uniform and non-uniform particle size affects the performance of the battery cells in different manner which was explained in the [19]. With the change in particle size, reduces or increase the interfacial surface area for reactions, affecting the porosity of the electrode, which affects the presence of the electrolyte in the electrode, thus a drop in useful capacity of the battery cell can be observed. The drop in capacity with respect to change in particle size can be observed in figs 2.16 and 2.17.The particle size of anode was varied randomly from $5 microns$ to $15 microns$, in an order from $PS1$ to $PS7$ respectively and the selected value is $PS5$, $12 micron$. The particle size of anode was chosen as anode consist higher amount of active material for the electrochemical reactions to take place in the battery cell [19].

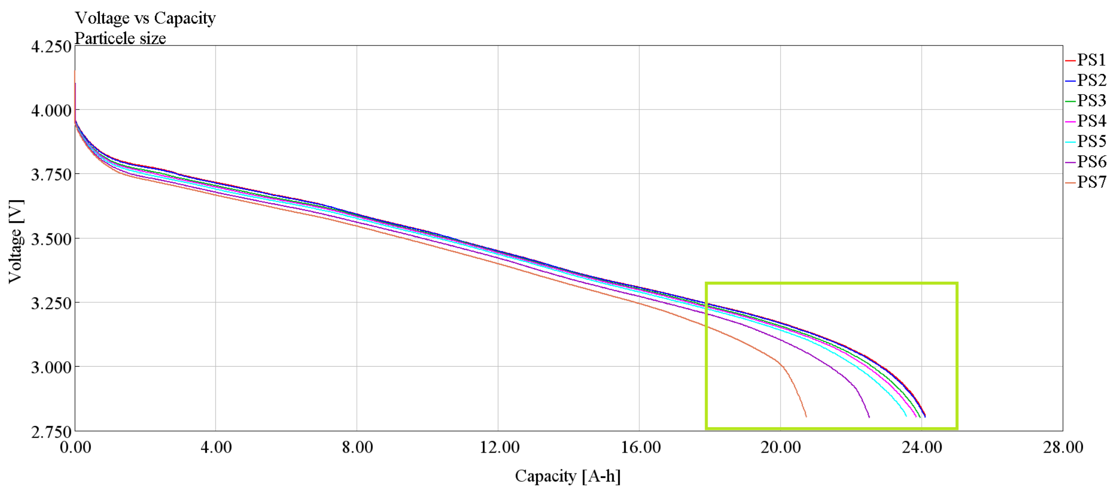

Figure 2.15: Change in capacity due to change in particle size

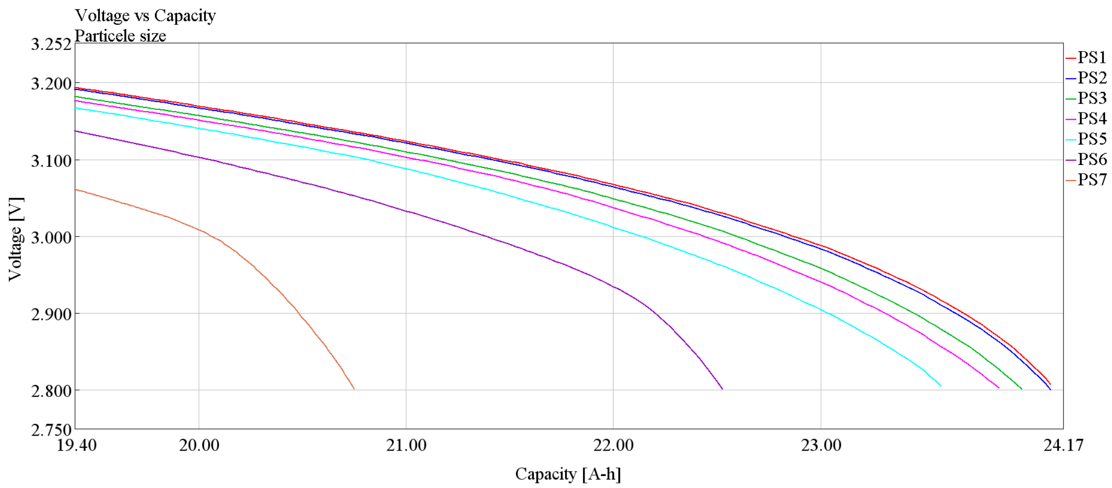

Figure 2.16: Zoom in - Green Box

2.4.4 Other parameters

Few parameters which couldn't be evaluated and have been taken from [9] are described briefly, as these parameters play important role in the intercalation/de-intercalation rate of the electrochemical model cell. The parameters like ionic conductivity, diffusivity do affect the porosity and tortuosity for the reactions to produce necessary results. Electrolyte effective ionic conductivity and electrolyte diffusivity is expressed as

$$\kappa^{eff} = \frac{\epsilon\kappa}{\tau} \tag{2.8}$$

$$D_e^{eff} = \frac{\epsilon D}{\tau} \tag{2.9}$$

where, ϵ is the porosity and τ is tortuosity and these two parameters affect the distance travelled by the Li^+ ion, so does its reaction rate within electrochemical model. These two parameters are related to diffusivity of the electrode and also helps in intercalation/de-intercalation of Li^+ ions while charging or discharging the battery cell [20]. For the electrochemical model, the important parameter is the battery cell temperature. It is important for the simulation, as per the Arrhenius law, the redox reaction rate gets affected by temperature, which means that with the change in cell temperature, the electrochemical properties of the cell do get affected. One of the drawback of electrochemical model is that the electrolyte concentration remains constant at lower current rate affecting the accuracy of the required results[15].

2.5 Why not 1D or 3D model ?

A 1D model relates to the mathematical modelling of the cell which exhibits the different characteristics in an electrochemical model due to transfer of the Li^2 ions between electrodes while charging or discharging the battery cell. And, according to 1D models, its operation depends on the concentration of active material in the electrodes and on the particles surface area C(x,t) whereas in the 2D model, the governing equations confirms that the solid phase concentration depends on a spatial 2D concentration $C_e(x, r, t)$, where x is the position of the particle, r is the radial position and t is time as shown in fig 2.17. Although, the 3D model provides efficient results of energy density, the temperature response inside the battery cell, overall heat generation and distribution inside the battery cell, it uses complex governing equations, and it is computationally time consuming [15].

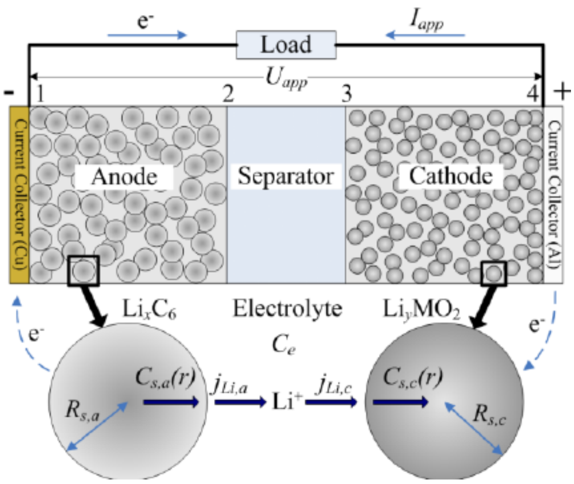

Figure 2.17: Schematic of $P2D$ Model - discharge process [2]

3
Control Strategy

3.1 PID control strategy

There are different control algorithms available to be used either in industries or applications. The Bang on/Bang off, PID, neural network and the fuzzy logic strategies. The controllers are also categorized into feed-forward and feedback controllers. The feed-forward controller sends an additional output to compensate for a known change whereas a feedback controller provides the result which can affect the next step as explained in [21]. In this thesis work, the feedback control system was implemented as a PID algorithm. The PID controller uses a closed-loop system through which it controls a certain parameter which was supposed to match with the ordered value, it is typically referred to as set-point. The PID controller uses the "difference" or "error" between the set-point and the resulting output value in every working loop [22]. This is a kind of mechanism which calculates the error in every cycle and gives a signal to the process to minimize the error [21]. In this work, the set-point is the reference surface temperature of the cell and the parameter to be controlled is the varying surface temperature of the battery cell, a block diagram for the closed-loop control algorithm is shown in fig 3.1.

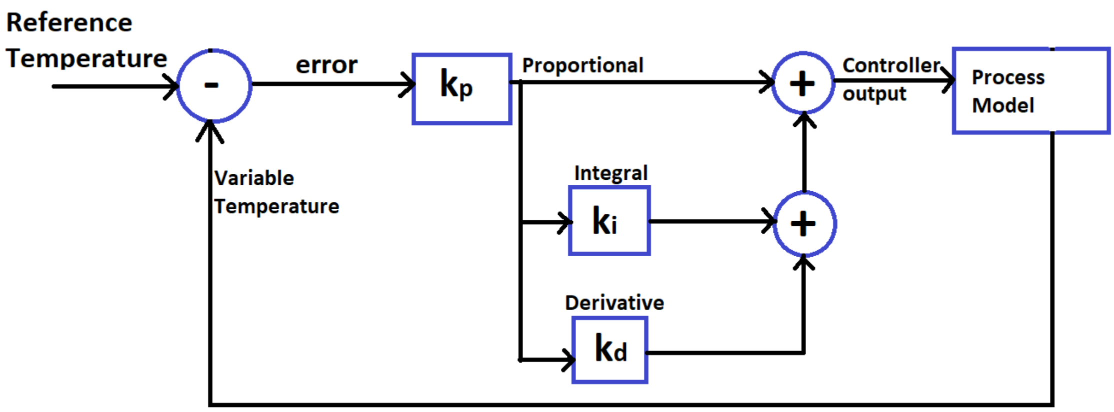

Figure 3.1: Block diagram for PID model

3.2 PID - parameter estimation

There are many methods available through which one can tune the PID controller parameters such as k_p, k_i and k_d gain values [23]. The Cohen-coon method is suitable when the system is an open loop system. For the closed loop feedback control system, the Ziegler-Nichols method is preferred to use for tuning of the PID controller parameters, as it can work for close loop system [22]. The Z-N method can be used for systems where there is a lacking mathematical description. [24].

To identify the individual gains k_p, k_i, and k_d, an algorithm was written in Python to find the parameters. An algorithm was developed which calibrated the necessary parameters such as the controller gain K_c, integral time, τ_i and the delay time, θ_d which resulted in finding and calibrating the proportional gain k_p, Integral gain k_i and the derivative gain k_d using eqns (3.1),(3.2) and (3.3).

$$k_p = \frac{1}{K_c} \tag{3.1}$$

$$k_i = \frac{k_p}{\tau_i} \tag{3.2}$$

$$k_d = k_p.\tau_d \tag{3.3}$$

The necessary tuning parameters of the PID controller are the controller gain K_c, the integral time constant τ_i, and the derivative time constant τ_d. The controller gain is in multiplication with the proportional error and the integral error. The integral time constant,τ_i must be positive and smaller so it can keep the integral term larger to contribute to the controller output signal and thus the derivative time constant τ_d should be positive. The strategy to estimate the parameters and the tuning method was explained in detail by [21]. The error value is formed from the difference between the set-point (SP) or reference temperature and the process variable (PV) or the measured temperature, shown by eqn (3.4) and (3.5).

$$e(t) = SP - PV \tag{3.4}$$

$$U(t) = k_p e(t) + \frac{k_p}{\tau_i}\int_0^t e(t)dt + k_p\tau_d\frac{d(PV)}{dt} \tag{3.5}$$

3.3 Parameters tuning

There are various tuning methods available to find the PID parameters [20]. In this thesis work, simple tuning method is used where θ_d i.e, the delay time has to kept zero and process time T_p was assumed equal to integral time τ_i, to estimate the required PID parameters such as k_p,k_i k_d. By using the python algorithm, we can calibrate the required parameters with tuning calculations such as,

$$T_p = \tau_i; \theta_d = 0 \tag{3.6}$$

The delay time θ_d, is the time difference between the response of the system after applying a input step pulse. The process time T_p, is a model parameter which helps in tuning the PID parameters. It represents the time taken by the process variable to reach 63.2% of the final change [21]. However, it was not estimated according to the developed algorithm, to keep the simple tuning of the parameters and secondly, to observe the sudden drop in battery cell temperature by reducing the delay time. So, it was assumed to be taken as equal to the integral time (τ_i) to reduce overshoots. Here, in order to re-find the parameters τ_d, K_c and τ_i, an adjusting fidget was designed and final values are presented in the estimated parameters Table 3.1.

Table 3.1: PID estimated parameters

Controller gain/ Time Constants	**Values**
Controller Gain (K_c)	0.20
Integral Time (τ_i)	3.01
Derivative Time (τ_d)	0.50

3.3.1 Steps to determine control gains

- After specifying the set point, the controller gain can be found by changing K_c to find the periodic oscillations in the result.

- Adjusting the process time T_p or integral time τ_i to reduce the oscillations, until they reach the steady state.

- And, following the standard parameters estimation find the relevant parameters for P, PI and PID.

- The influence of the individual parameters was observed by changing the necessary parameters and controller gains, such as K_p, K_i and K_d and K_c based on the work [25].

4

Experimental Setup

4.1 Case Setup

In this chapter, the test equipment is explained along with illustrations and relevant calibrations. The general equivalent test setup and procedure is briefly explained. The test setup consists of a GAMRY Booster to provide current up to 30*Amps*, this current high enough to generate such a high loss that a temperature change can be observed. An ice-chamber is used as a water reservoir that can produce the cold water. The Shenchen pump has an inbuilt flow meter to control the flow of the water in the cooling plates. The water flow rate will vary with respect to change in temperature to mitigate the generated heat. The Shenchen pump is controlled with pulse width modulation (PWM) 0-5Volts output, using an Arduino UNO board with our own program. The Arduino UNO also collects the measured surface temperature of the battery cell through K-type thermocouple sensors, Arduino MEGA reads the inlet and outlet water temperature since heat loss are determined by the differences between these two temperatures. The experimental test setup shown in fig 4.1.

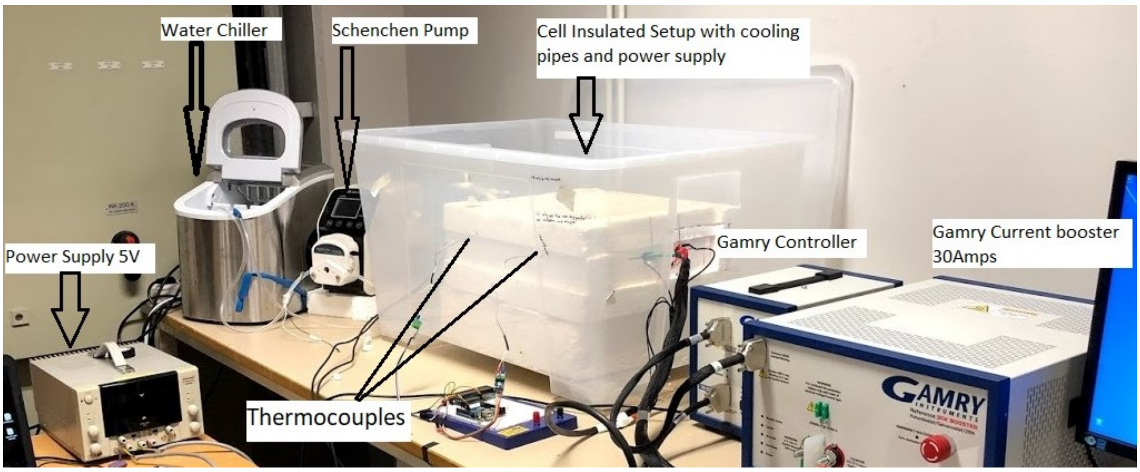

Figure 4.1: Experimental test setup

4.2 Test Setup Equipments

4.2.1 GAMRY Reference 3000 (30A)

A GAMRY Reference 3000 and 30k booster is used for charging and discharging the battery cell. The booster can provide a maximum of 30 A as charging and discharging current.

4.2.2 Temperature Measurement

The battery cell surface temperature is measured by a K-type thermocouple which has a range of measuring from $-75 to +1000$ °C with an accuracy of 0.5°C. Regarding the coolant, the water temperature is measured with a PT100 water temperature sensors which can measure temperatures from -50 to +125 °C with an accuracy of $(0.3 + 0.005t)(°C/W)$.

4.2.3 Arduino UNO and Arduino MEGA2560 Micro controllers

Two separate Arduinos are used in this setup. An Arduino UNO is programmed to control the cooling management system of the battery cell while an Arduino MEGA2560 is used to measure the inlet-outlet water temperature. Both these devices are user-friendly due to the Arduino Micro controller's open-source library which makes it easier to understand and to fulfil the requirements.

4.2.4 Pump

A Shenchen Lab N6 is a peristaltic pump, it is used to control the flow rate of water and it has a operating range of $0.007 - 1330 mL/min$. The Shenchen Pump has an inbuilt control system through which the flow rate can be controlled. It is a 220V AC pump but also has a DC operating mode (+5V and +10V) which is used for this setup.

4.2.5 Climatic Chamber for HPPC Test

Climatic Chamber KK-115. This chamber can achieve a temperature range from -10(°C) to +60(°C) and a relative humidity from 30-90% [3]. We have done the tests using a Styrofoam box developed in a previous work[3] so hole sizes are the same, the chamber is an adiabatic chamber so that all heat inside don't go out in the environment, the cables used are for giving power to battery cell as mentioned in section 4.2.1, other cables are connected to the Aduino-UNO and there are temperature sensor cables attached to the LIB in the test setup.

4.3 Calibration

4.3.1 Calibration of shenchen pump

The Shenchen pump was calibrated by controlling the flow rate, measuring 200ml of water flowing into a beaker for 1 minute. The manual calibration was confirmed by repeating the step with a different range of volume of water. Later in the thesis work the flow rate was chosen to maintain the surface temperature of the battery cell close to a fixed reference value while charging-discharging the cell and to reduce the power loss as well. The linear relation between the required flow rate according to the power loss is shown in fig 4.2.

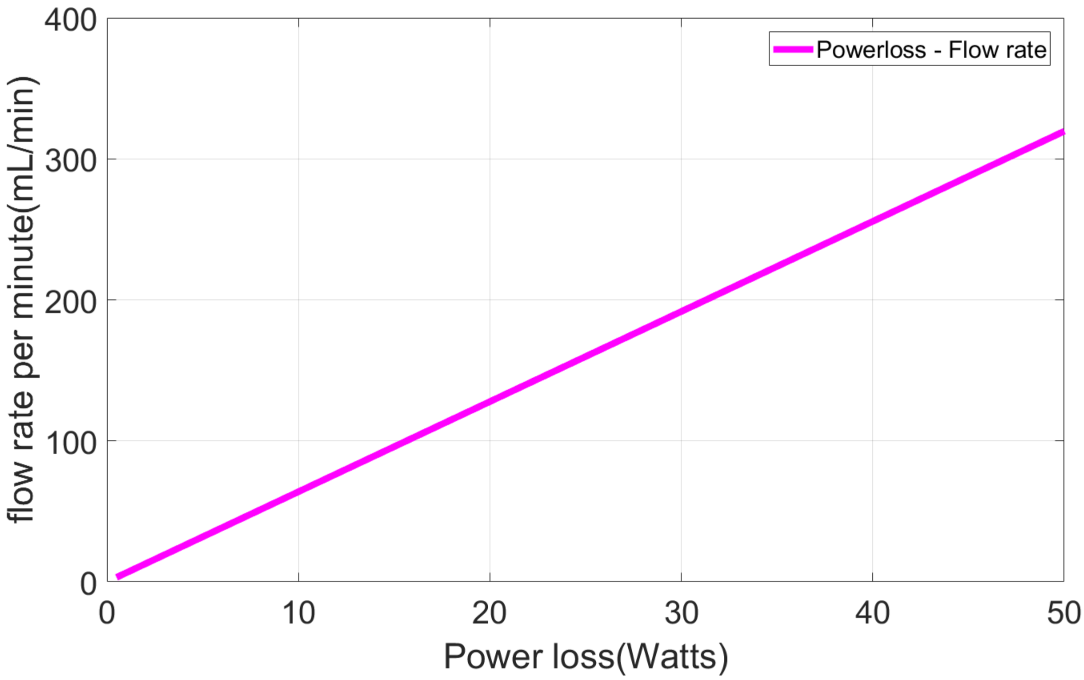

Figure 4.2: Calculated flow rate for the power loss

4.3.2 Calibration of PT100 sensors

PT100 sensors are used to measure the water temperature entering and leaving the aluminum plates whilst performing charging-discharging of the battery cell. These sensors are calibrated at the lowest flow rate of 12.5ml/min as well as for a higher flow rate of 200ml/min.

5

Cooling System

5.1 Physical Test Setup

In this section, a descriptive explanation is given about the cooling setup of the physical battery cell.

5.1.1 Dummy Test Setup

During the dummy test, a dummy cell is considered which consists of an aluminum plate and a resistance carpet and this dummy cell have the same size as the Li-ion battery cell. The Dummy cell is presented in fig 5.1 and it was placed between two cooling aluminum plates. When power is supplied to the resistance carpet, it warms up the aluminum plate. The surface temperature of the dummy cell was measured by an Arduino UNO using K-type thermocouple sensors. A control algorithm in the Arduino micro-controller compares the measured temperature with the reference value and if the measured value is higher than the reference value, then the Arduino orders the pump to operate by sending a pulse width modulation (PWM) signal. The pump has a calibrated flow meter which controls the water flow in the aluminum cooling plates to maintain the surface temperature of the dummy cell at a fixed reference value. For the final test, the dummy cell was replaced with the battery cell and the procedure was repeated.

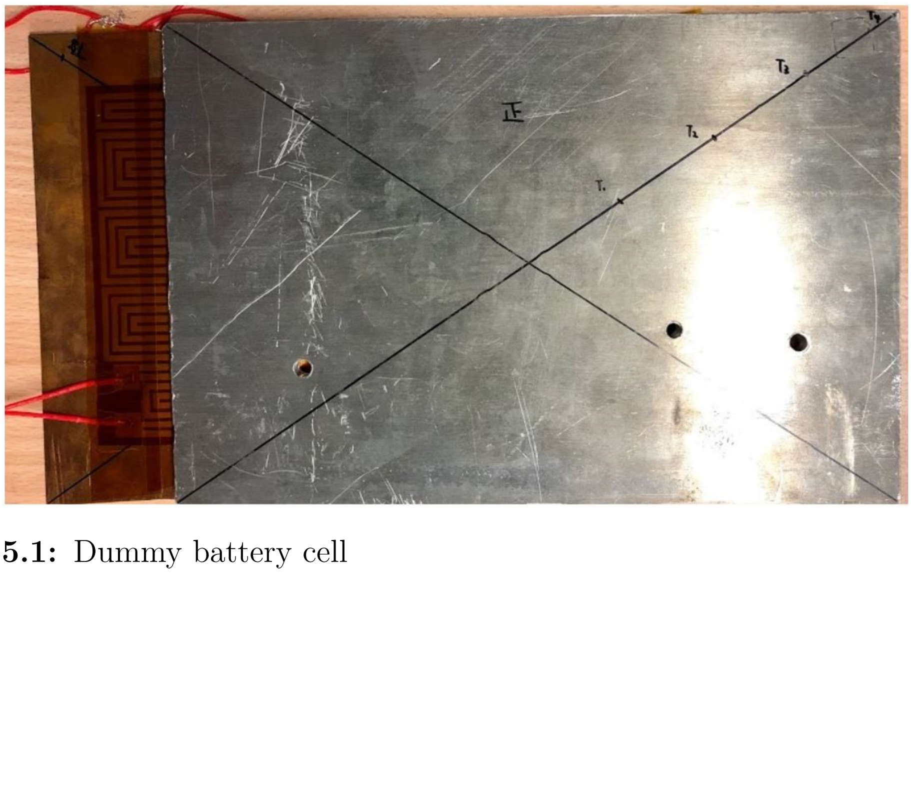

Figure 5.1: Dummy battery cell

5.1.2 Control with the PID algorithm

A PID algorithm is written in Arduino, compared the surface temperature with the reference temperature, in order to control the flow of the water in cooling plates. When the measured surface temperature gets higher than the reference temperature the Arduino-UNO outputs the pulse width modulation (PWM) signals which are fed to the DC pump to control the flow rate in accordance with the variation in the surface temperature of the cell.

5.1.3 Cooling Plates

Although, there are different cooling options executed or proposed in the automotive industries [20],[26]. The liquid cooling method is implemented in this thesis work. The design of the cooling plates is described in and for the cooling purpose, the flow rate was not fixed, it vary according to the surface temperature of the battery cell, thats why the flow rate is not defined as laminar or turbulent. The designed cooling plates used are shown in fig 5.2

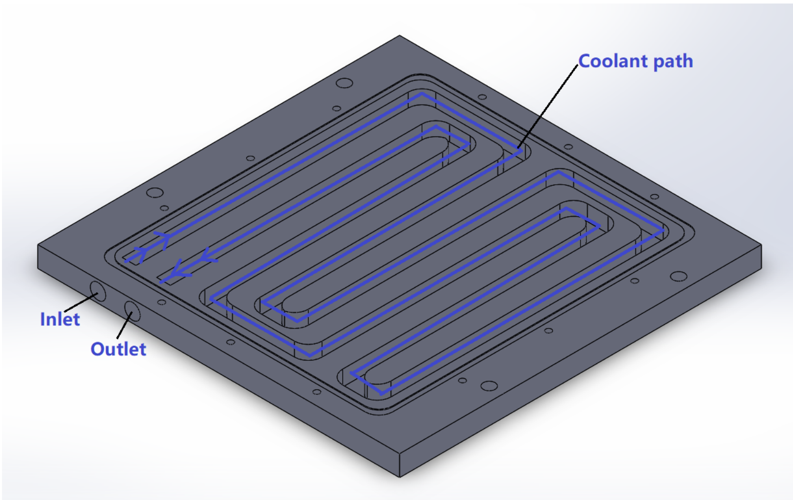

Figure 5.2: Tubing of the cooling plates [3]

5.1.4 Battery cell test setup

Two K-type thermocouple sensors are placed in the middle of the cell and close to the cathode terminal as shown in fig 5.2. assuming surface temperature homogeneous except near the positive tab. After placing the sensors, the battery cell was placed between the cooling plates, and this assembly (fig 5.4) was placed in the Styrofoam box from [3] which has a high thermal resistance, to trap the heat generated during charging-discharging of the battery cell.

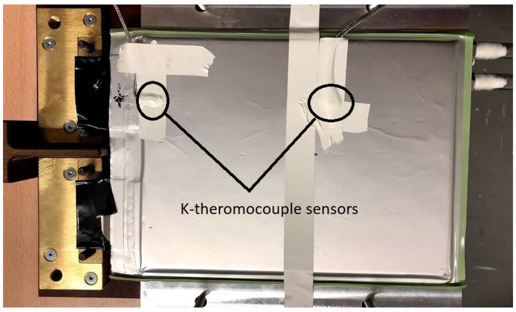

Figure 5.3: Sensor position

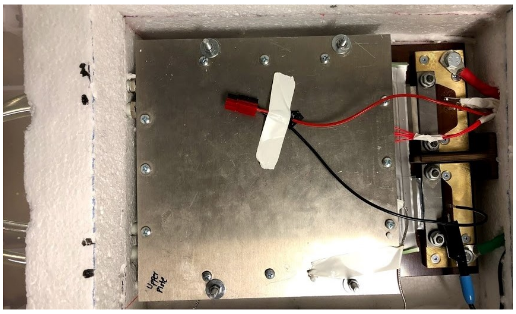

Figure 5.4: Cooling plates - Test setup

5.2 Control circuit for cooling system

During this thesis work, one of the aims is to develop a mechanism to control the battery cell temperature to a desired value. In order to fulfill the purpose, a control algorithm was implemented in Arduino which worked efficiently with the help of the Arduino open-source library. This algorithm made to pump to operate whenever the surface temperature of the cell differs from the reference value and controls the water flow in the aluminum plates, so that the heat generated by the battery cell can be absorbed, to maintain the battery cell surface temperature. The generated heat as well as the increasing surface temperature of the battery cell are minimized by the PID method. The control circuit for the cooling system is presented by an equivalent electrical circuit in figure 5.4.

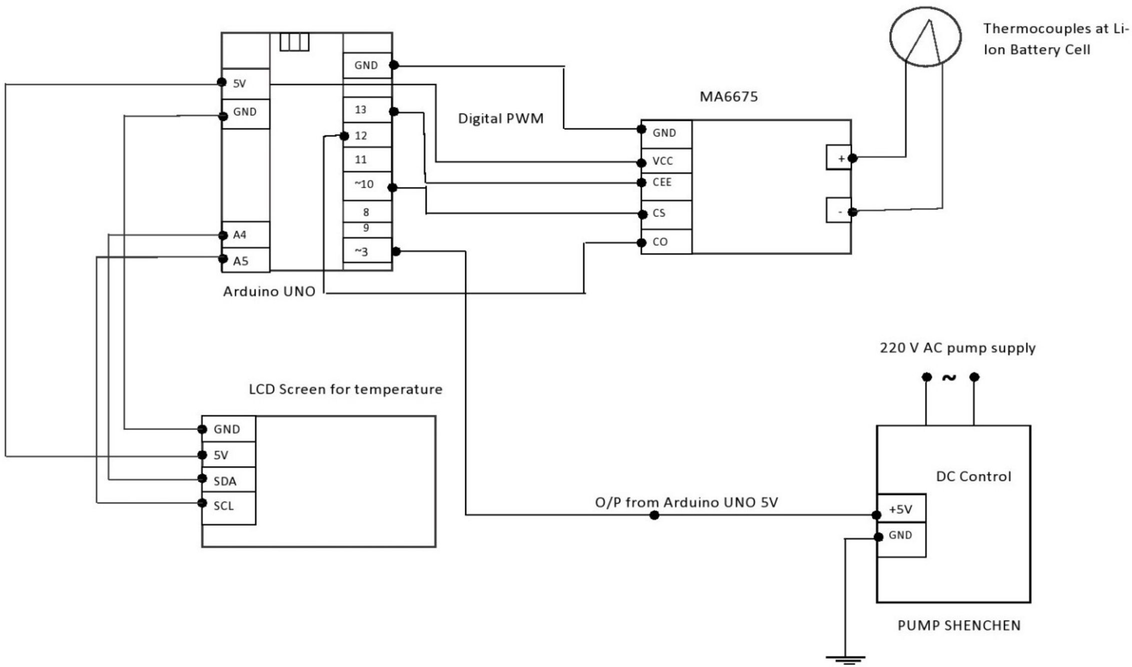

Figure 5.5: Electrical circuit for arduino based cooling system

5.3 Cooling system performance

To evaluate the cooling system performance, the cell was discharged and charged continuously with 26$Amps$ and the temperature response of the battery cell was measured without and with cooling respectively. This test is done by continuously charging-discharging the cell with high current to develop a cycle, which can elevate the cells' temperature with continuous high-power consumption.

5.3.1 Battery cell temperature

Using the same test setup as shown in fig 4.1, the battery cell was discharged and charged with GAMRY Booster with 1C-rate, thus the battery cell losses generated heat, which resulted in a change in the surface temperature of the battery cell.

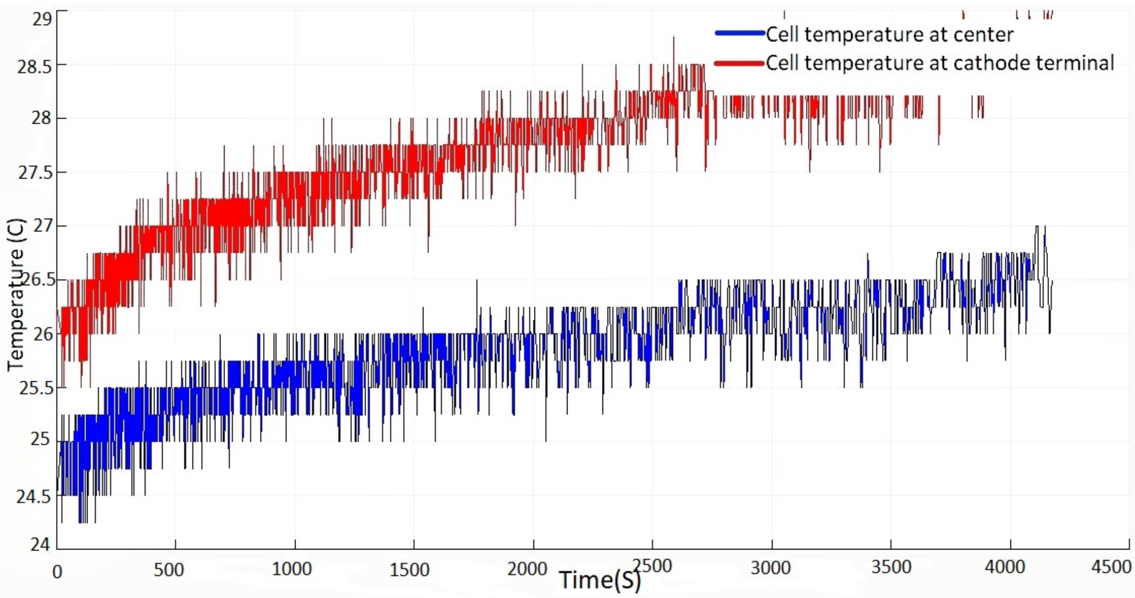

Figure 5.6: Battery surface temperature without cooling at 1C-rate,test setup according to Fig 5.4

Fig 5.6 shows the temperature response of the battery cell when the cooling system was disabled. There are two different temperature are shown in fig 5.6, which were measured at cathode terminal and at the center of the battery cell represented by red and blue curves respectively.The measured temperature at the cathode terminal is higher than the temperature measured at center of the battery cell, since at the cathode terminal, an inherent oxide aluminium film on the current collector acts as an auxiliary cathode [3].

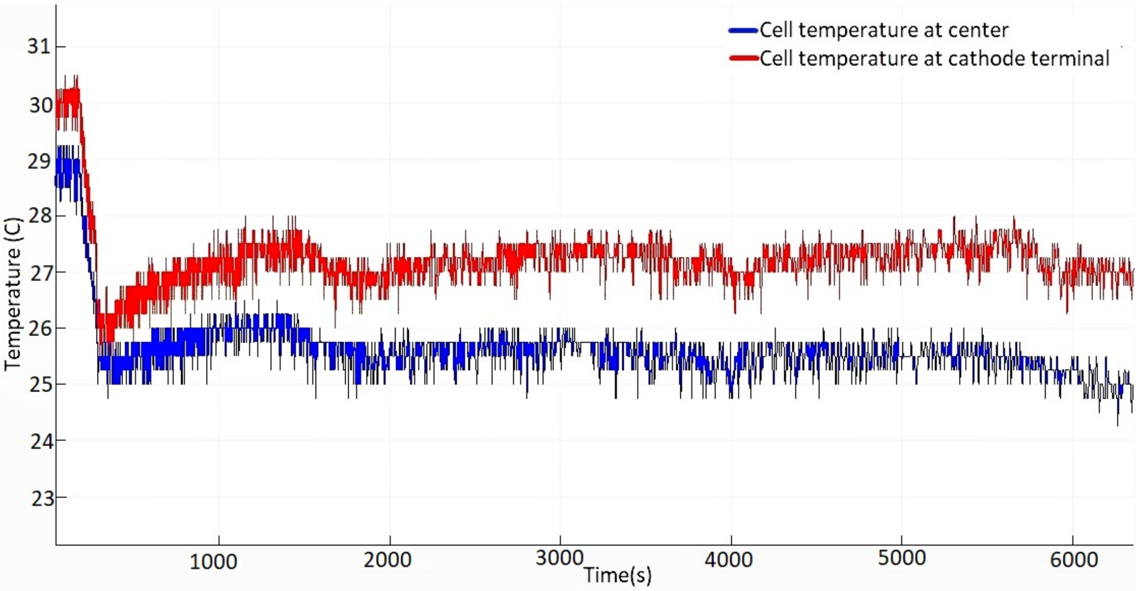

Figure 5.7: Battery surface temperature with cooling at 1C-rate and reference temperature set to 27°C, test setup according to Fig 5.4

After enabling the cooling and setting 27°C as reference temperature, the result of the implemented control can be seen in fig 5.7. The surface temperature of the battery cell was raised by charging and discharging it and by immediately switching ON the pump to allow the cold water to flow in the cooling plates at t=200s, the surface temperature of the battery cell was brought down and later maintained constant around the reference temperature of 27°C. During charging-discharging of the battery cell the surface temperature was fluctuating and the water flow rate in the aluminum plates was following the change in temperature to absorb the heat generated by the battery cell and kept the battery cells' surface temperature constant throughout the cycle.

5.3.2 Battery cell thermal RC parameters

A MATLAB/Simulink model was designed to extract the thermal R and C values. The thermal model of the cell was assumed to be of first order as presented in by [11] and were used as in (2.3). R_{th} and C_{th} are the parameters of the thermal model, where 'R_{th}' stands for thermal resistance which determines the difference between the initial and final surface temperature of the cell whereas 'C_{th}' stands for thermal capacity of the battery cell which defines the dynamic nature to understand the transient event.

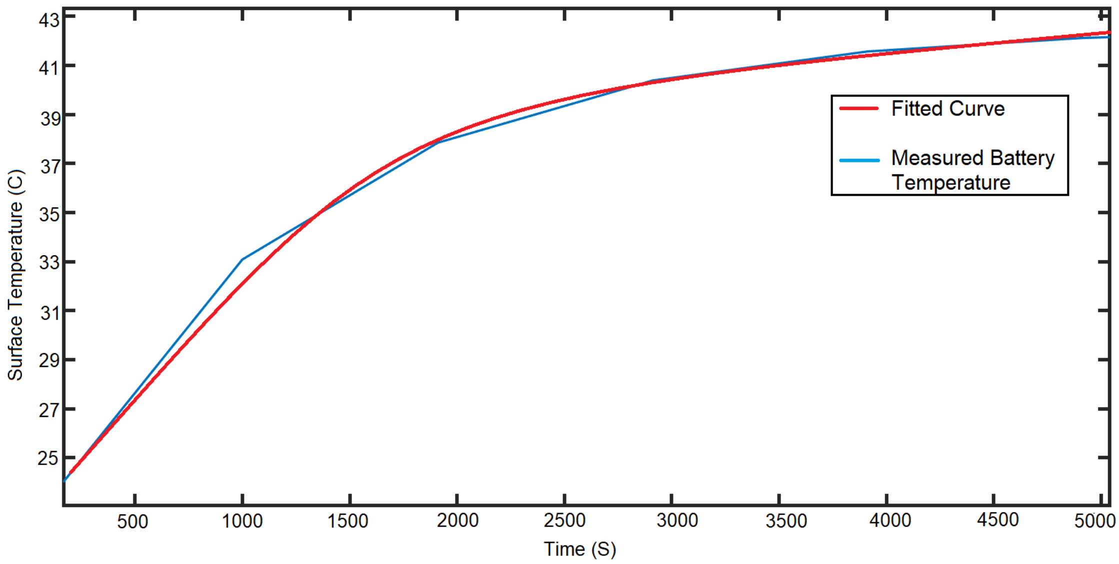

Figure 5.8: Fitted curve with actual surface temperature of the battery cell

And, the thermal $R_{th}C_{th}$ value are calculated by using a non-liner least square curve fitting method on the temperature data curve obtained while discharging the battery cell disabling the cooling system, the measured R_{th} and C_{th} values are 2.29K/W and 3324 J/K respectively for test setup presented in fig 5.4. The value of convective resistance was a reference value calculated in previous work [27]. These thermal $R_{th}C_{th}$ parameters were used in MATLAB model to achieve the desired results which could verify the theoretical results.

5.4 MATLAB/Simulink Models

In this section, two Simulink models are presented. The Simulink models are designed to calculate the temperature rise in the battery cell. In Fig 5.8 and fig 5.9 Simulink models are shown which represent the electro-thermal model of the battery cell without and with the cooling system respectively. In fig 5.9, the control algorithm implemented in cooling mechanism is represented by the PID block and transfer function block consists the thermal R_{th} and C_{th} values which were estimated by using Non-linear curve fitting method, which helped to achieve the desired simulation temperature results.

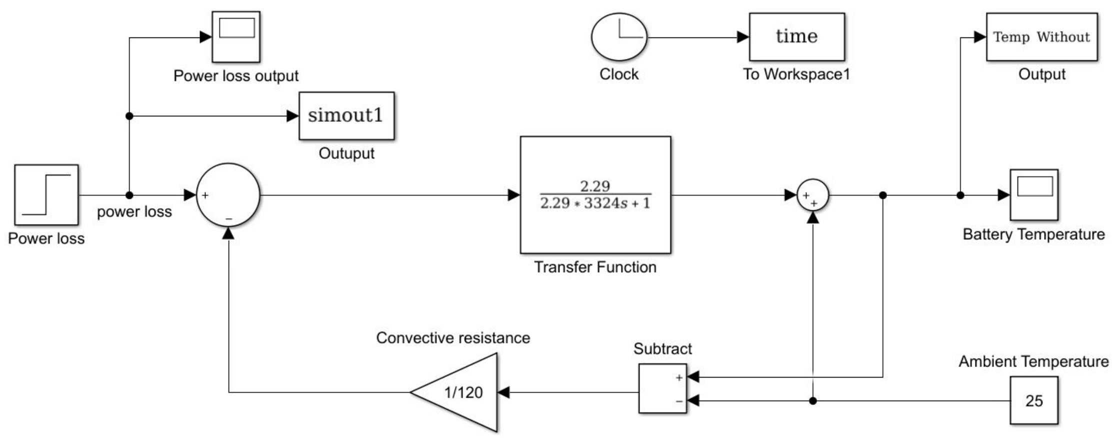

Figure 5.9: Theory model setup of the battery cell without cooling system

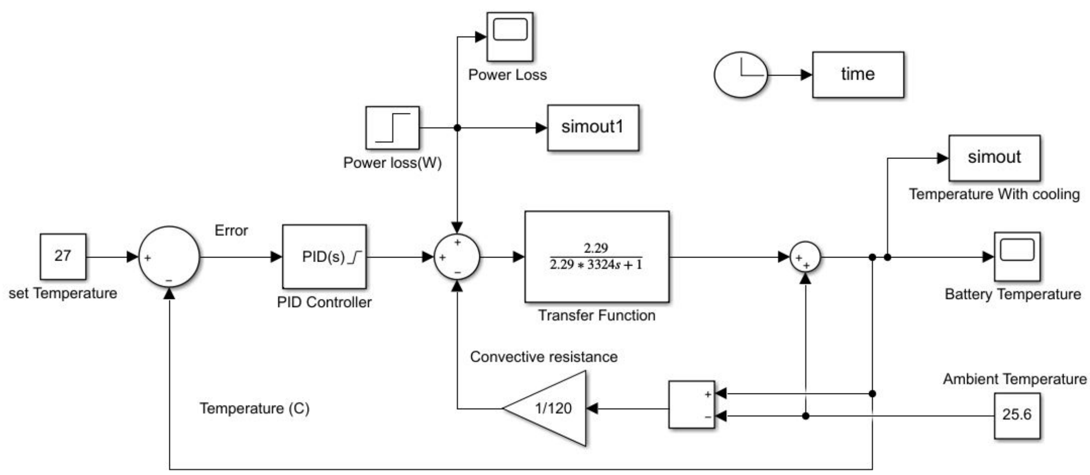

Figure 5.10: Theory model setup of the battery cell with cooling system

5.4.1 Comparison between experimental cooling system and MATLAB model

In this section, the results from the experiment and the Matlab model are compared. In fig 5.10 and 5.11, the Matlab model and theoretical test setup results without enabling the cooling system are presented. When comparing both results, the Matlab model curve is found to be a close representation of the experimental results, shown by the curves for both cases. The Matlab result reached to a similar value which was obtained by the cathode terminal temperature. For theory model, the temperature was set to 29 (°C) to mimic the physical test.

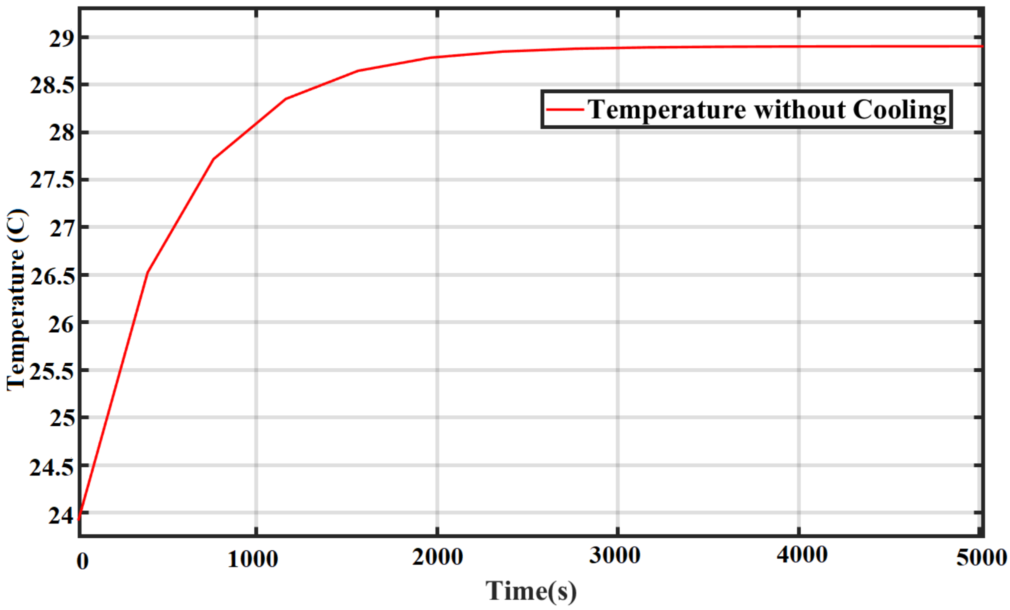

Figure 5.11: Simulation result for battery surface temperature without cooling

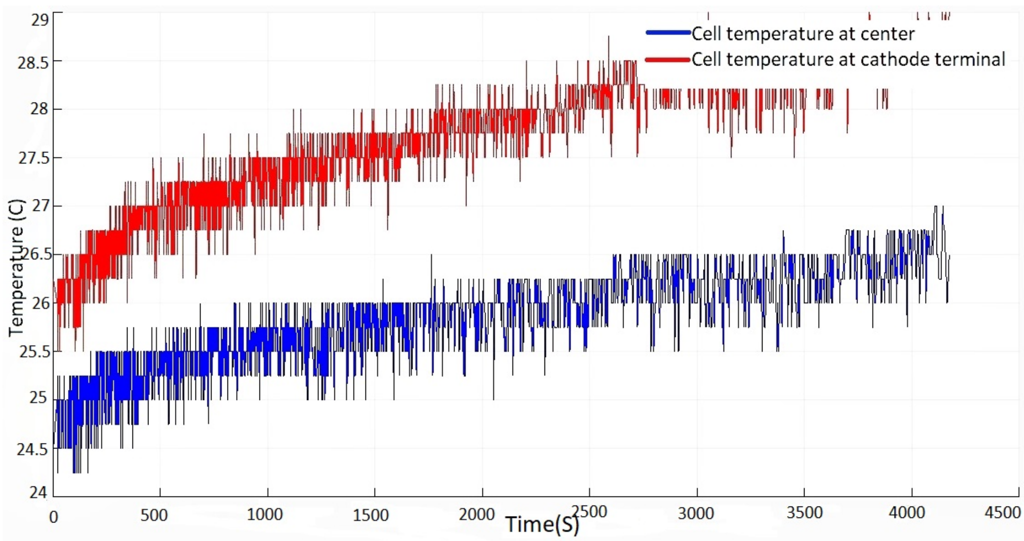

Figure 5.12: Battery surface temperature without cooling for test setup as in fig 5.4

Similarly, the results obtained from the above-mentioned models, including the cooling system and enabling the PID algorithm are shown in figs 5.12 and 5.13. The rise time for the simulated model is lower than the measured time for the theoretical results. And, for this category, the reference temperature was set to 27°C, so with the help of the control algorithm the surface temperature of the battery cell was controlled to be close to the reference temperature.

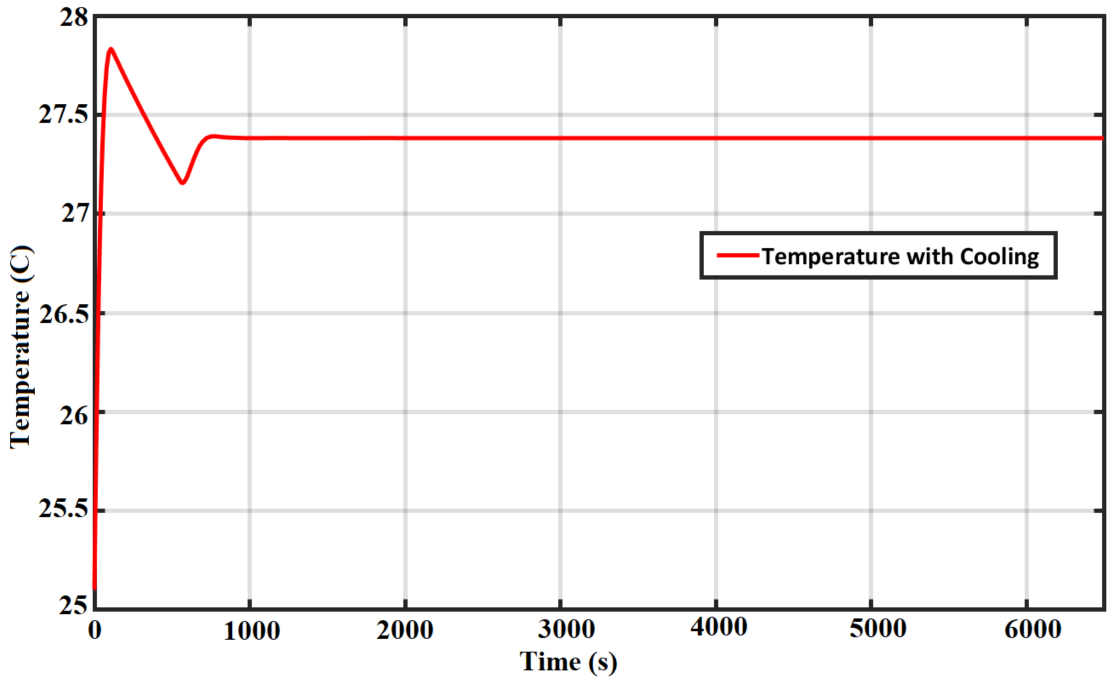

Figure 5.13: Simulation result for battery surface temperature with cooling system

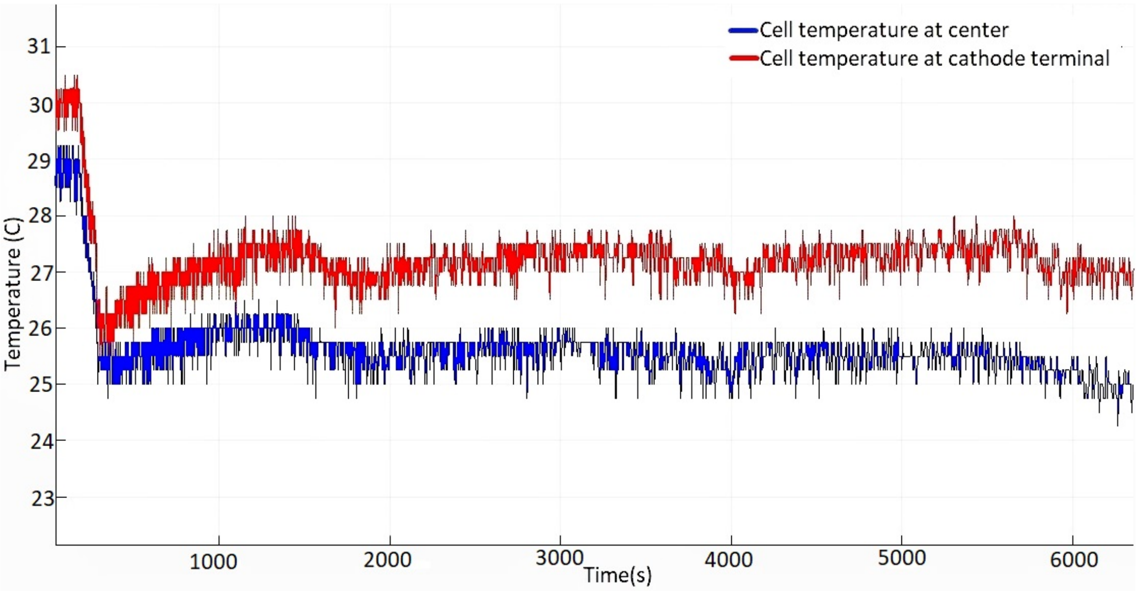

Figure 5.14: Battery surface temperature with cooling and reference temperature set to 27°C, test setup according to Fig 5.4

There is a difference in rise time of the individual simulation results indicating that the calculated thermal resistance 'R_{th}' and thermal capacity 'C_{th}' for both models are approximately same in nature. The measured rise time for the theoretical test setup was 0.001 (°C)/sec and calculated rise time for the simulation model was 0.0005 (°C)/sec.

Table 5.1: Rise Time of individual model

Model Type	**Rise Time**
Theoretical - Physical Model	0.001 (°C)/sec
Matlab - Simulink Model	0.0005 (°C)/sec

5.5 Power loss calculation

Power loss of a battery cell is calculated using an adiabatic chamber to compare and verify the theoretical value $2.028W$ with the experimental result. There are different ways to calculate the power losses of the cell during a charging-discharging cycle as discussed in [28], but in this work the calorimeter method is used the similar test setup as described earlier. It works on the principle of thermodynamics law.

5.5.1 Battery cell power loss

Styrofoam has a resistivity of $0.033W/(m.K)$ calculated by [3] with insulated cotton covering the battery cell to prevent the internal heat from evacuating out in the environment or getting the case setup affected by the environment surrounding it. Theoretically, the $26A$ leads to a battery cells' resistance of $3m\Omega$ [3], which leads to a power loss of $2.02W$. So, to verify the similar loss, the battery cell was charged and discharged for more than an hour at 1C-rate i.e $26Amps$. During the process, the battery cell generated heat which was measured by an K-type thermocouple and due to generated heat the measured inlet and outlet water temperature has a difference which was measured and shown by red and blue curve respectively in fig 5.15. In order to mitigate the power loss, the required flow rate of water was estimated by using (2.6) and the similar test setup was used as explained earlier in chapter 4.

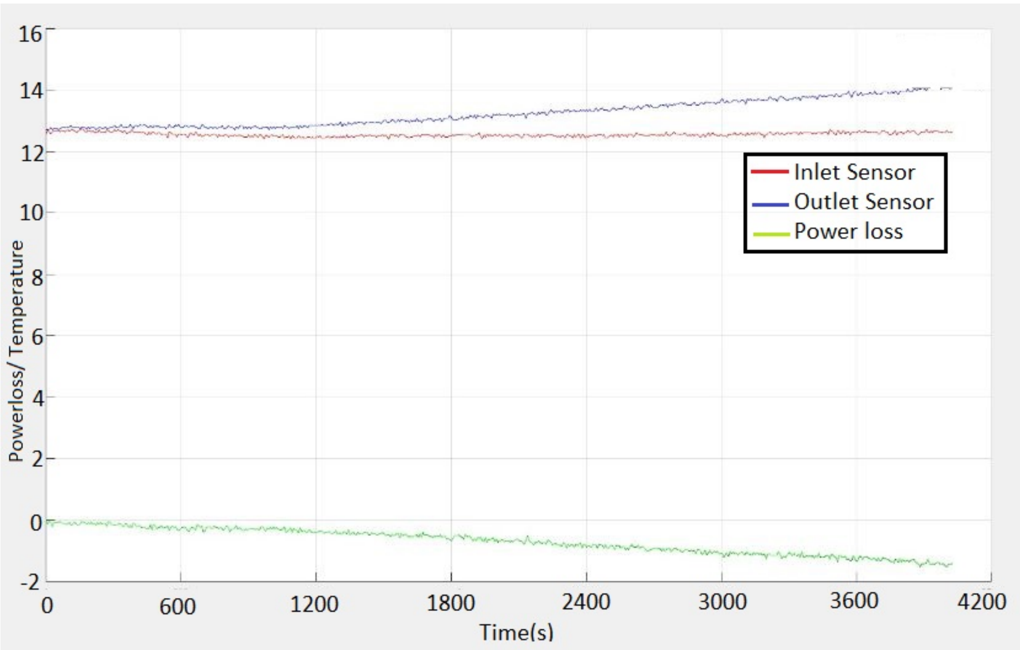

Figure 5.15: Measured power loss with temperature difference to calculate the flow rate

The measured value was approximately $2W$ and the other two curves represent the the inlet and outlet water temperature of the cooling plates which were used to calculate the required flow rate, which can absorbed or mitigate the generated heat while charging and discharging the battery cell.

5.6 Specific Heat Capacity

The specific heat capacity was calculated using the adiabatic calorimetric environment following the second law of thermodynamics which states, entropy in a closed system increases.

5.6.1 Test procedure

The specific heat capacity was calculated for the Li-ion battery cell used in test setup in fig 5.4. The test setup along with enabled cooling mechanism was used to capture the specific heat capacity of the battery cell. After switching ON the test setup, the specific heat capacity of the battery cell was measured by monitoring the change in the surface temperature of the battery cell i.e, ΔT_b from fig 5.14, while charging and discharging it from t=200 sec to t= 1500 sec, considering the estimated power loss, Q_{loss} from fig 5.15 and the mass of the battery cell M_b[9]. The heat released by the battery cell i.e, Q_{loss} is the energy absorbed by the water flowing in the cooling plates i.e, Q_w following the second law of thermodynamics. Therefore, the specific heat capacity (C) is calculated by

$$C = \frac{Q_{loss}}{M_b \Delta T_b} \tag{5.1}$$

Table 5.2: Values for the parameters used in estimating specific heat capacity

Parameters	**Estimated Values**
Q_{loss}	$1.90W$
M_b	$550g$
ΔT_b	$2.5K$

The specific heat capacity of the Li-ion battery cell is calculated to be $1.39J/g.K$. The specific heat capacity of the battery cell will differ with the different chemistry type of battery cell used in the experiment. The estimated value is slightly higher than the expected result but it is not surprising as different measuring methods will produce different specific heat capacities. The specific heat capacity of the LIB is estimated using calorimetry method including a cooling control mechanism and the thermal capacity of the battery cell was identified by using open loop system i.e by charging and discharging the battery cell continuously, then observing the rise in temperature and applying a non-linear curve fitting method, which provided thermal RC parameters. This is why, the specific heat capacity of the battery cell differs from the former thermal capacity.

6

Electrical Model

6.1 Parameters Estimation

The lithium-ion battery cell used in this project is represented by an $R0+2RC$ ECM. This model can predict the battery transient behavior. At various SOC levels the RC parameters differs due to changes in the internal impedance of the battery cell and to estimate these $2RC$ parameters of the ECM, the battery cell voltage behavior was observed with changes in applied current as performed by [29]. To estimate the RC parameters, data is required in the form of either charging or discharging pulse curves which are referred as hybrid pulse power characterization (HPPC) curves, this is an iterative process including repetitive estimation of data using MATLAB simulation.

6.1.1 Pulse test to estimate dynamic parameters

Data obtained from charge pulse test such as in fig 6.1 and 6.2, provided required data to study the dynamic behavior of the battery cell at different SOC levels.

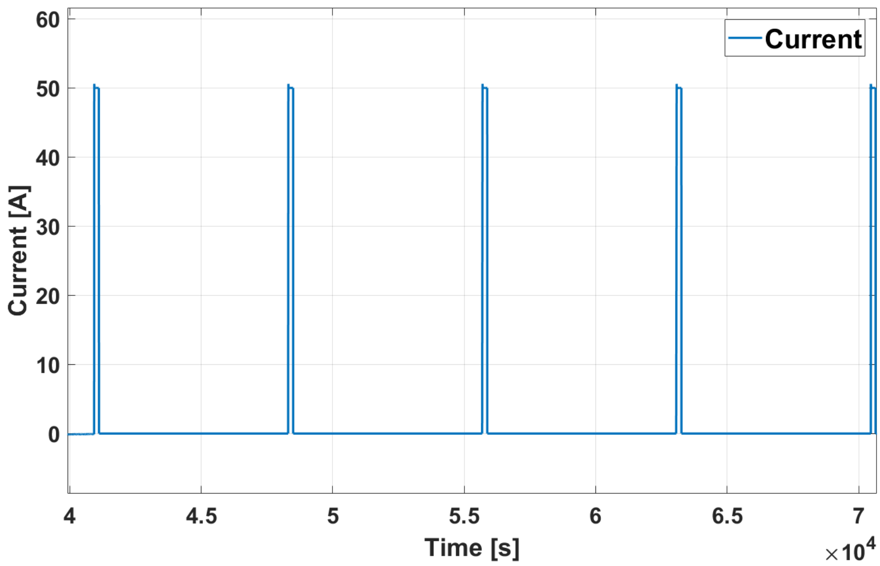

Figure 6.1: HPPC current profile

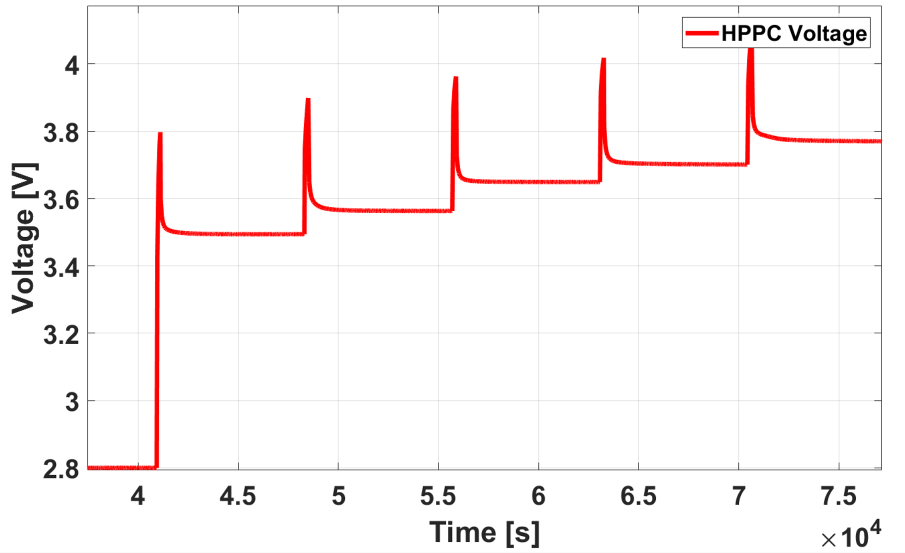

Figure 6.2: HPPC Voltage profile

Fig 6.3, presents a closer look at a single pulse, indicating the open circuit voltage (OCV) and the circuit's dynamic behavior at a given SOC level. The pulse reached to the steady state every time before starting a new pulse. However, there was a relaxation period of a few hours before the next pulse and the RC parameters are estimated by implementing a nonlinear curve fitting algorithm on the relaxation period.

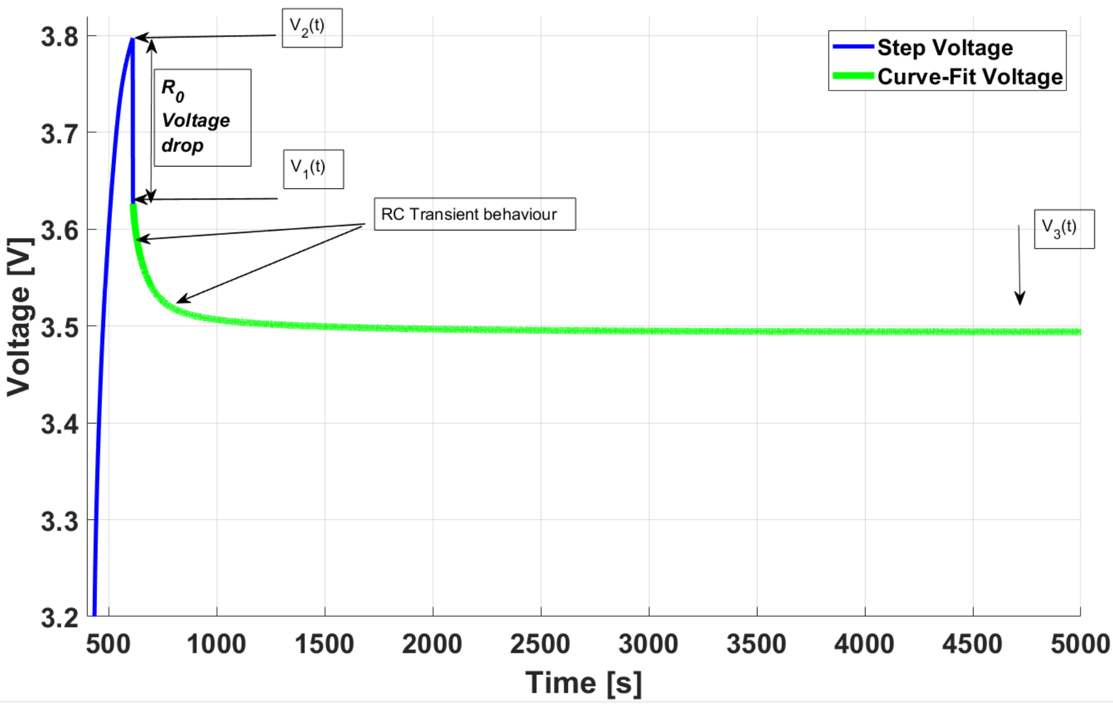

Figure 6.3: HPPC Voltage profile

6.1.2 Parameters estimation method

Due to the ohmic resistance, the change in battery cell voltage occurs as soon as a step current is applied, so the ohmic resistance can be calculated as

$$R_0 = \frac{v_2(t) - v_1(t)}{I} \tag{6.1}$$

where $V_1(t)$ is the voltage when a charge pulse initiated, $V_2(t)$ is the voltage decrease after the charge pulse ended, I is the applied current. And, the other $2RC$ parameters was identified by implementing non-linear curve fitting method in MATLAB on the greener part in fig 6.3. The relaxation period voltage $V_f(t)$ was identified on the basis of previous work[ref] exhibiting the dynamic behavior,

$$v_f(t) = v_3(t) + X1 * \exp(^{-}Y_1 * t_{pulse}) + X2 * \exp(^{-}Y_2 * t_{pulse}) \tag{6.2}$$

where $V_3(t)$ is the voltage of the relaxation curve, X1, X2, Y1,Y2 are the coefficient used to obtain the results after setting their initial values respectively. And, the following equation were used to represent the co-relation between these coefficients and respected parameters

$$\tau_1 = \frac{1}{Y_1}; \tag{6.3}$$

$$\tau_2 = \frac{1}{Y_2}; \tag{6.4}$$

$$R_1 = \frac{X_1}{I * (1 - \exp -Y_1 * tpulse)} \tag{6.5}$$

$$R_2 = \frac{X_2}{I * (1 - \exp -Y_2 * t_{pulse})} \tag{6.6}$$

From these relations, τ_1 and τ_2 represents the time constants for R_1C_1 and R_2C_2 respectively and t_{pulse} is the time duration of the current pulse, which is different for the two data sets used in this project work respectively.

6.2 Estimated Parameters

The estimated RC parameters at respective SOC levels representing the dynamic behavior are shown in following figures.

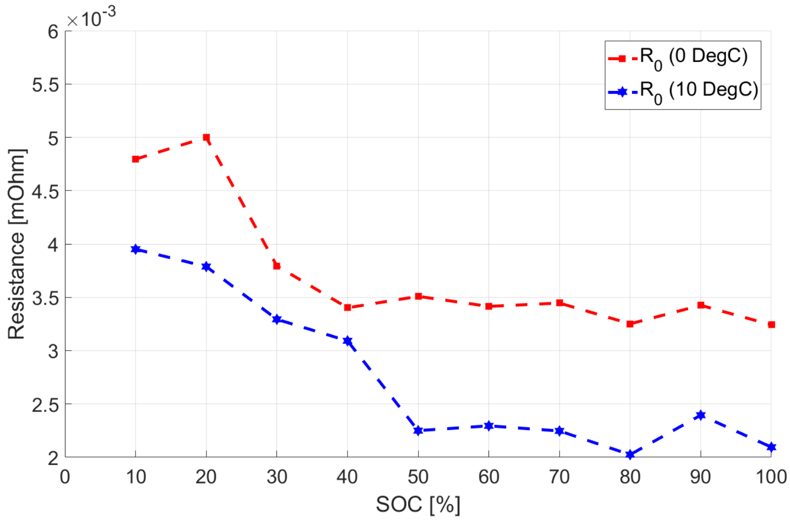

Figure 6.4: R_0 Internal Resistance Parameter at different SOC level

Fig 6.4, shows the R_0 results which are calculated using (6.1), which presents that the internal resistance fluctuates along with the SOC levels and due to the battery cell temperature as well. Secondly, R_0 decrease with an increase in ambient temperature from 0(°C) to 10(°C). Although, it should remain approximately constant after initial drop, which shows that the function made up to calculate the parameters was inconsistent.

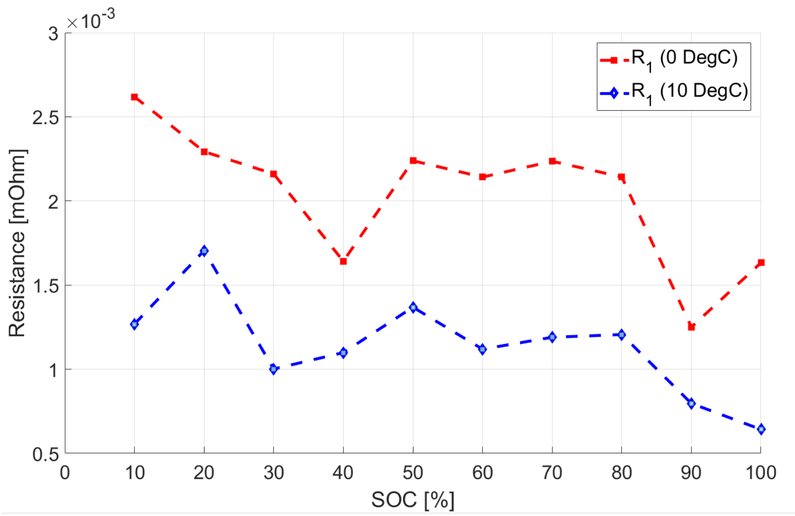

Figure 6.5: R_1 parameter at different SOC level

The R_1 parameter result is shown in fig 6.5, it can be observed that R_1 have the similar general trend as for R_0, it fluctuated and decreased at a higher SOC level. However, the trend for both the curves are similar.

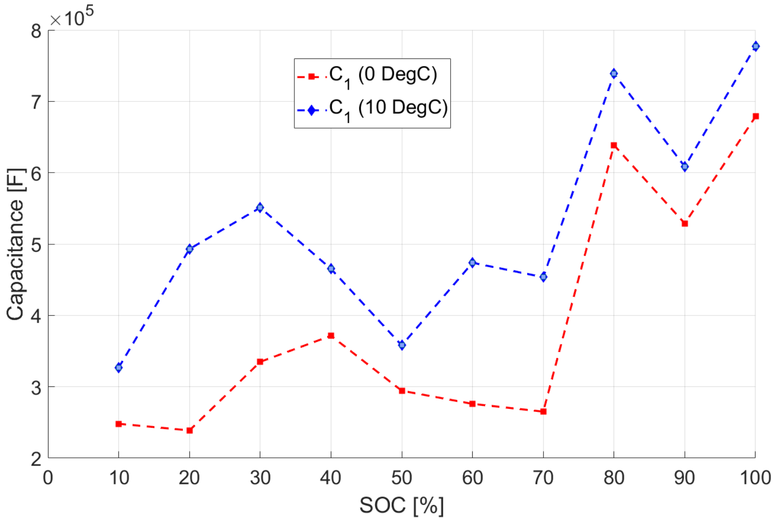

Figure 6.6: C_1 parameters at different SOC level

In fig 6.6 the parameter C_1 of the ECM can be observed which shows that C_1 increase with SOC levels as well as it increases with an increase in ambient temperature.

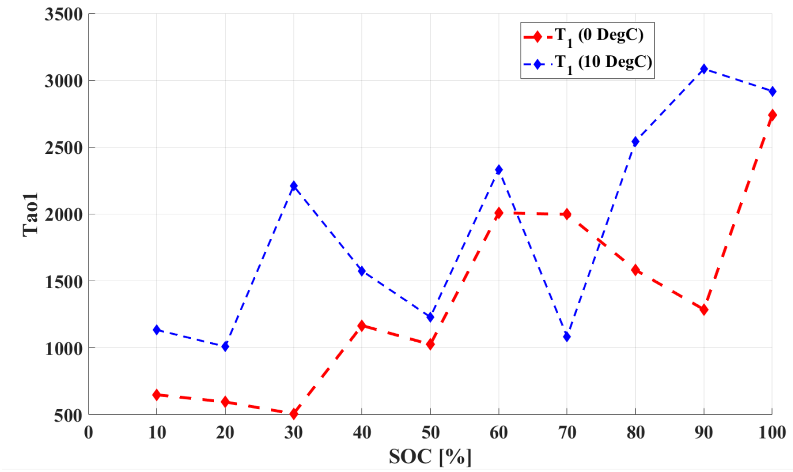

Figure 6.7: τ_1 time constant for different SOC level

The slower time constant for the $2RC$ circuit is presented by τ_1 in fig 6.7 which represents the time constant for the first link of the ECM. The slow time constant is fluctuating in nature as well as slightly decreasing along with the variation in SOC levels. Fig 6.8 presents the R_2 parameter results which shows that R_2 increases with their respective SOCs and depict similar decreasing trend as R_1, which is a result of an improper curve fitting, however, the trend was similar for the R_2 resistance for both temperature.

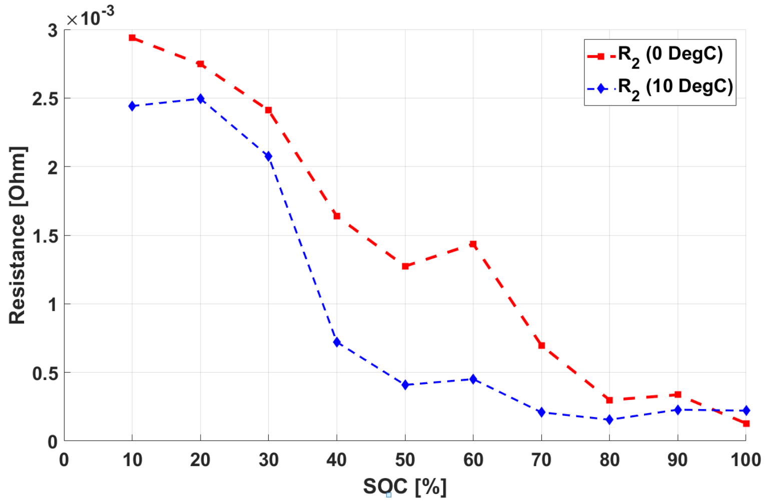

Figure 6.8: R_2 parameter with different SOC level

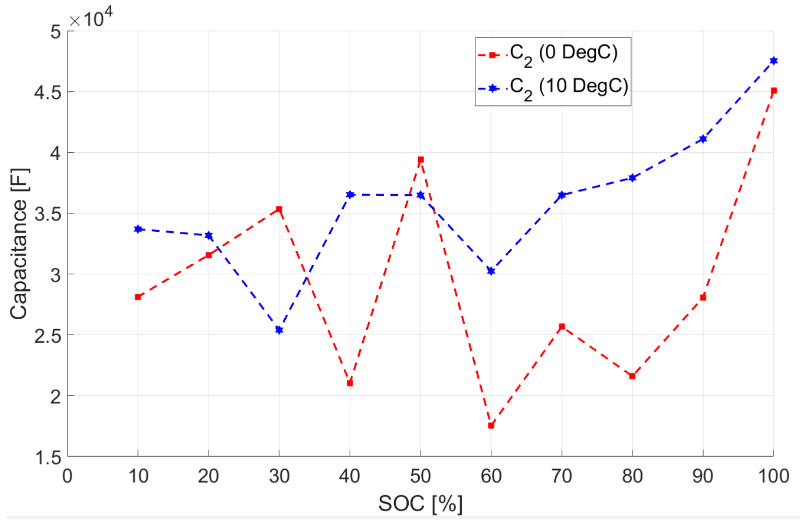

Figure 6.9: C_2 parameter with different SOC level

The C_2 parameters are shown in fig 6.9. The general increasing trend is similar to C_1. The capacitance for 0(°C) consist higher fluctuations than the capacitance at 10(°C). Although, the C_2 parameters increases at higher SOC level but the capacitance C_2 parameters increase with increase in temperature.

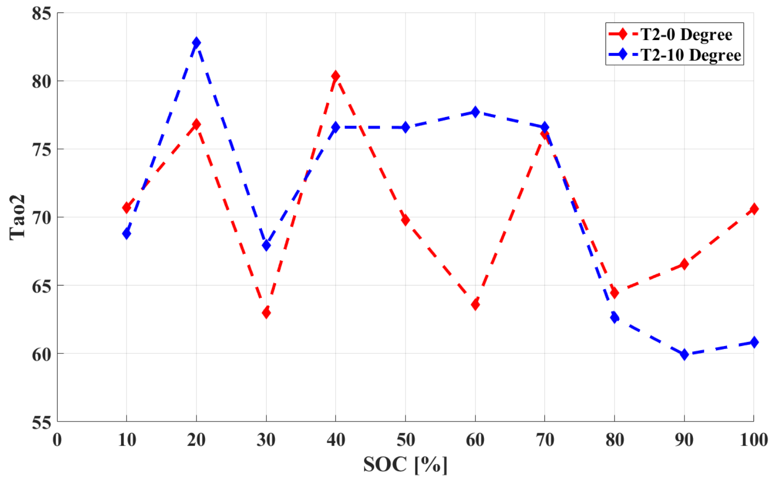

Figure 6.10: τ_2 parameter with different SOC level

The faster time constant for the second RC link of the 2RC-ECM represented by τ_2 is shown in fig 6.10 exhibiting the decreasing trend although, it is fluctuating for both temperatures.

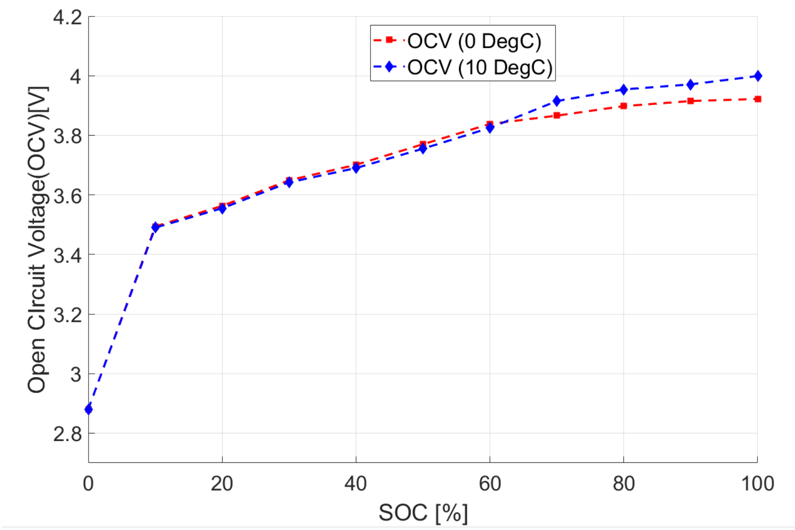

Figure 6.11: OCV at different SOC level

The OCV with variation in SOC is presented in fig 6.11 for different temperatures, which shows that a similar trend till 60% SOC level, but at higher SOC level the OCV profile for 0(°C) is lower than that at 10(°C).

7

Electrical model Results

7.1 GT-Suite-AutoLion Results

The $2RC$-ECM is a representation of the battery cell to estimate the parameters but to validate the electrical model, an electrochemical battery cell model was developed in GT-Suite-AutoLion considering the battery cell dimension, chemistry, thermal behavior and several other parameters accumulated from previous literature work. To estimate the $2RC$ electrical parameters, a HPPC current profile was utilized in the electrochemical model to collect the data and to identify the required RC parameters.

In fig 7.1, the HPPC Control block is shown to represent the HPPC current profile used to charge the model cell and the Lithium-ion battery cell block is an electrochemical model representing the battery cell.

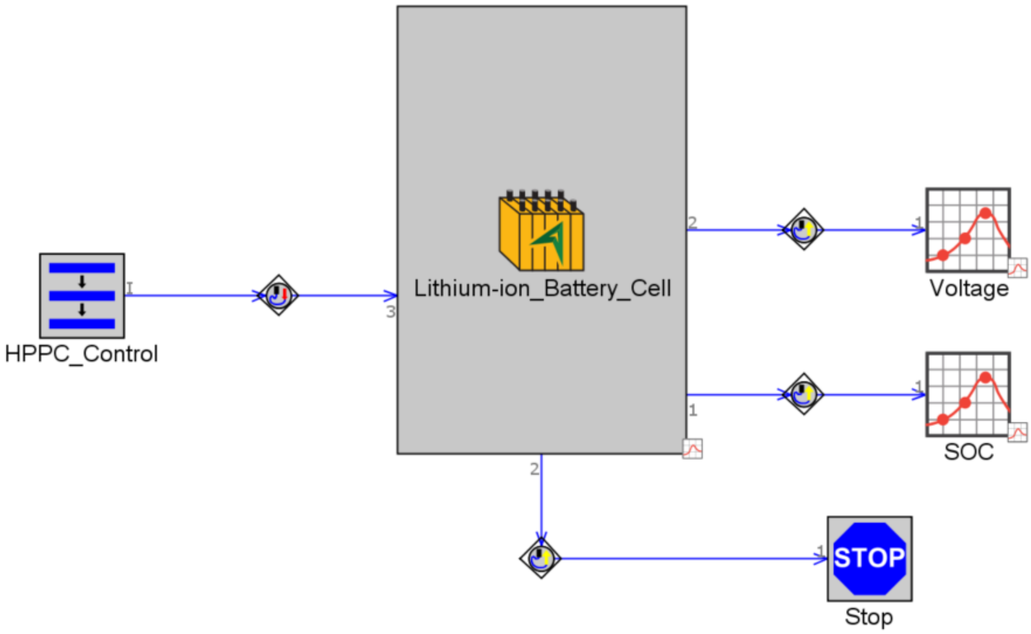

Figure 7.1: AutoLion battery validation model

7.1.1 Estimating Parameters - GT-Suite-AutoLion

The experiment was conducted with two different ambient temperatures of the battery cell - 0(°C) and 10(°C) in the climatic chamber. Similar conditions were designed in the validation model to maintain the battery cell temperature around the specific ambient temperature. An electrochemical model cell parameters were estimated and compared with experimental test parameters in the result analysis chapter. GT-Suite-AutoLion model also used a conventional approach, that is, the "Non-linear least square curve" method on the voltage profile to evaluate the parameters. The relaxation curve from the AutoLion model is presented in fig 7.2.

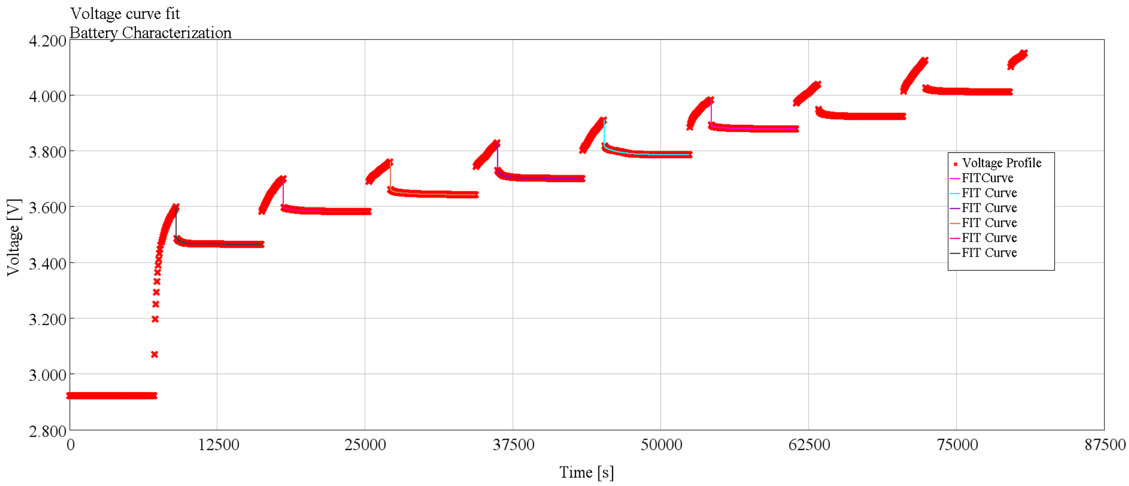

Figure 7.2: Relaxation curve of GTSuite AutoLion Model

7.2 GT-Suite-AutoLion - HPPC Profile Validation

After identifying the $2RC$ parameters, a model was developed to validate the HPPC voltage profile to confirm the accuracy of the AutoLion model. In fig 7.3, a validating model is shown, which compares the experimental voltage profile and AutoLion model result after using the same HPPC current profile in both models. The HPPC current profile used in both models was obtained from the experimental test.

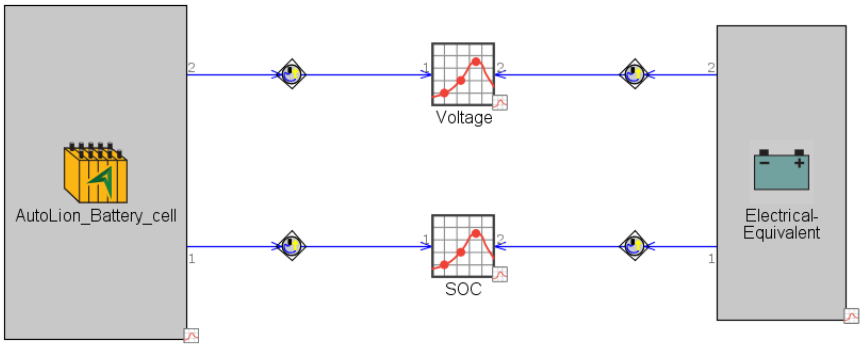

Figure 7.3: HPPC voltage profile validation model

The profile validation model consists of two separate models, AutoLion battery cell and Electrical equivalent model as shown in fig 7.3. The AutoLion battery model is an electrochemical model representing the physical battery cell and the electrical equivalent model consists of the battery equivalent-Thevenin circuit consisting of OCV, internal resistance and an optional number of RC branches for electrical dynamics. Each of the circuit parameters is the function of SOC, temperature, and current through the battery's terminals.

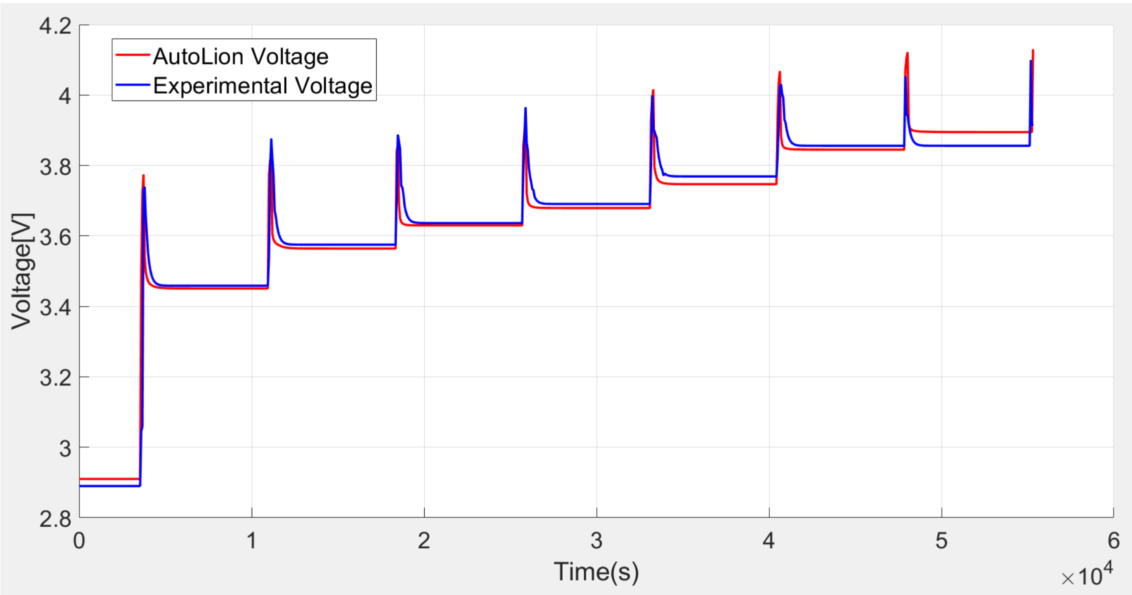

Figure 7.4: HPPC validated voltage profile

In fig 7.4, two overlapping curves represent a comparison of AutoLion and experimental results. The validation model stopped the simulation earlier, as it reaches the upper cutoff voltage limit sooner than expected. While validating the profile, the difference in the HPPC voltage profile is due to missing parameters in the AutoLion model as discussed in the theory chapter and might be due to incorrect measurement of experimental parameters. Besides those parameters, calendar aging of the battery cell is also not included while validating the results. So, parameters such as cell aging, cell degradation, cell film resistance, and SEI layer growth are unknown, which are also neglected making the modeled cell to be considered as a newly manufactured battery cell.

The primary effect of the battery cell degradation is an increase in its internal impedance, which was measured by the voltage drop in response to the load and the increase in internal impedance leads to a decrease in the charge capacity of the battery cell, since the higher voltage cutoff reached sooner than expected while charging the battery cell.

7.3 GT-Suite-AutoLion Optimization Model

To optimize the electrochemical model, it is important to ensure that the AutoLion battery model precisely replicates the physical battery cell performance, which is done by matching the HPPC OCV profile of the modelled cell with the experimental results by using the optimization model shown in fig 7.5.
The Optimization model is like a closed-loop function that works to improve the next value and the developed model utilizes all the selected parameters. These parameters were placed in the optimization model to minimize the RMS error between the experimental OCV and the Simulation OCV. The comparable results with these parameters and with few additional parameters are discussed in chapter 8. And, the initial default parameters which helped in the cell balancing and the OCV curve matching are presented in table 7.1.

Table 7.1: Parameters used in GTSuite-AutoLion Optimization Model

Parameters	**Description**	**Unit**
Capacity Loading	Cathode Loading	mAh/cm^2
N over P	N/P ratio	Fraction
Graphite$_{FCC}$	First Charging Capacity	mAh/g
Graphite$_{FDC}$	First Discharging Capacity	mAh/g
LMO$_{FCC}$	First Charging Capacity	mAh/g
LMO$_{FDC}$	First Discharging Capacity	mAh/g
NCM$_{FCC}$	First Charging Capacity	mAh/g
NCM$_{FDC}$	First Discharging Capacity	mAh/g
OCV$_{FULL}$	Open Circuit Voltage	V

7.3.1 Optimization Model

The optimization response depends on the chosen variables to reach to a steady state, comparing the experimental and the simulation result

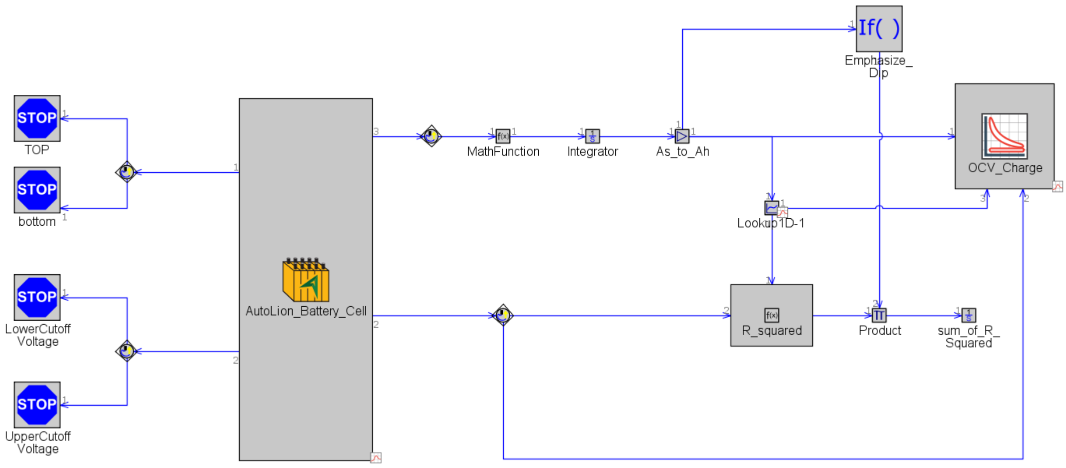

Figure 7.5: OCV matching and optimization model

8

Analysis

8.1 Comparison of simulated result with estimated parameters

In this chapter, estimated parameters from the experimental test and the simulation test are compared considering similar parameters, battery cell dimensions and charge capacity (Ah) but parameters such as ionic conductivity, ionic diffusivity, entropic heat, exchange current density, cell degradation were not considered, which inevitably restricts the electrochemical model to provide results close to the parameters obtained from experimental method. This is the comparison to understand the accuracy and strength of the developed GT-Suite-AutoLion model.

8.1.1 R_0 Internal Resistance over SOC and Temperature

The test was performed at two different cell temperatures, different data sets exhibiting similar characteristic trends were captured but the battery cells' internal resistance changed with the temperature which is shown by other works as well[**?**]. In fig 8.1 and 8.2 experimental and simulated results are compared, which shows a similar trend of R_0 decreasing with SOC but with an increase in temperature, the internal resistance R_0 decreased.

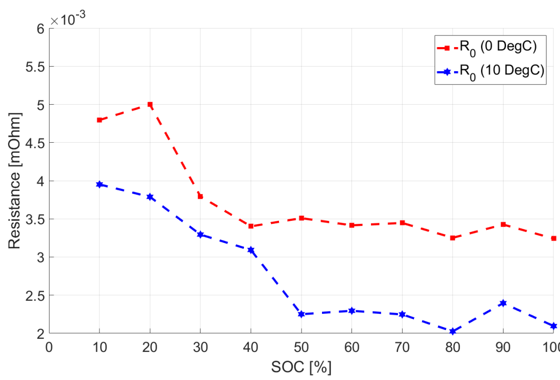

Figure 8.1: Experimental R_0

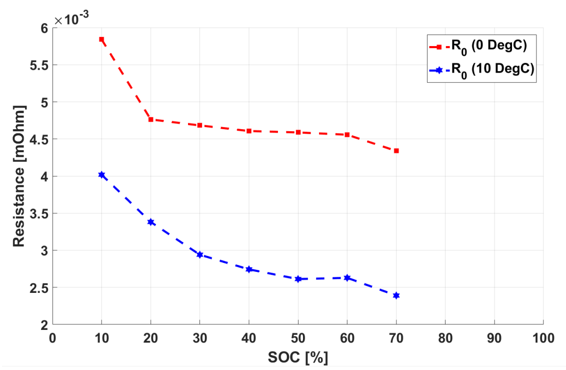

Figure 8.2: AutoLion R_0

8.1.2 Diffusion parameters behavior

The battery cell's diffusion behavior were represented by $2RC$ parameters of the ECM. The four parameters R_1, R_2, C_1, C_2 were estimated and identified for the $2RC$ ECM by both methods as described earlier.

By comparing Fig 8.3 and fig 8.4, the variation in the R_1 resistance parameter of the ECM can be observed. The results obtained from the two different methods have different fluctuating trends but these parameters decrease with increasing SOCs. Besides the general trend, the results don't have the same nature because the time constants associated with both models are different. Time constant depends upon the values of R and C which are different in both comparison figures, as Experimental values are higher, because of high resistance which is due to usage, charging-discharging cycles, therefore electrolytes concentration changes so the battery resistance increases mainly during discharging. (The discharge resistance is higher than the charge resistance as the discharge reactions are exothermic (releasing heat) at low SoC). The loss of electrolyte is also a frequent cause of increased electrolyte resistance.

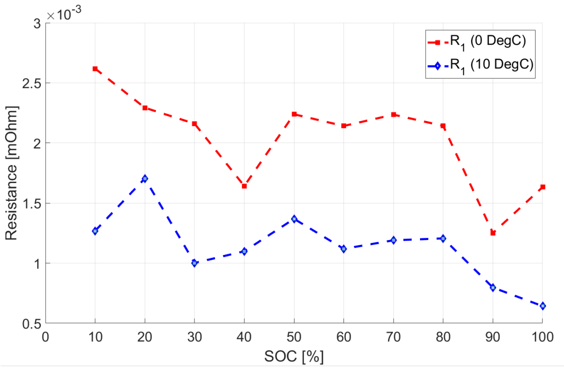

Figure 8.3: Experimental R_1

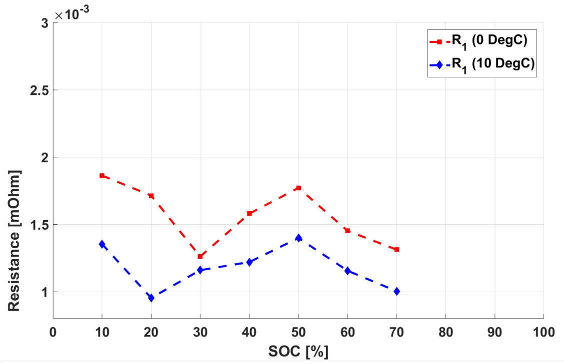

Figure 8.4: AutoLion R_1

In fig 8.5 and fig 8.6 the decreasing nature of the R_2 parameter is compared, the general trend of experiment and AutoLion based parameters have decreasing trends with the increasing SoCs. The resistance is lower at a higher temperature.

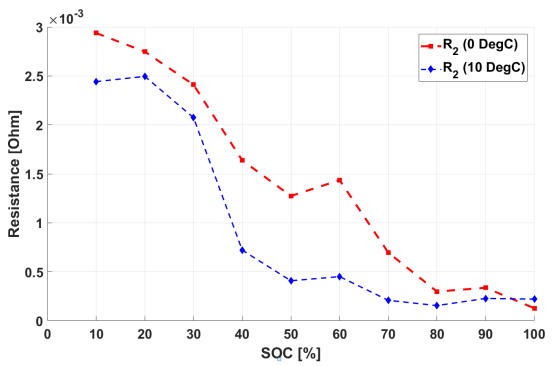

Figure 8.5: Experimental R_2

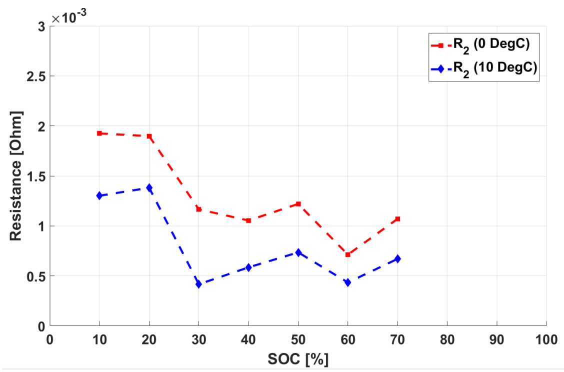

Figure 8.6: AutoLion R_2

The capacitance C_1 parameters from two different method have unlike fluctuating trend, although, these two results exhibits the similar rising trend at higher SOCs as shown in fig 8.7 and fig 8.8.

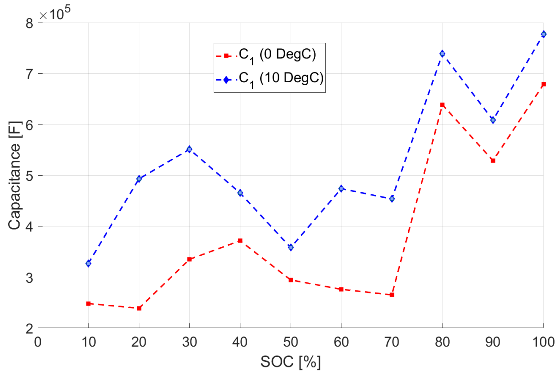

Figure 8.7: Experimental C_1

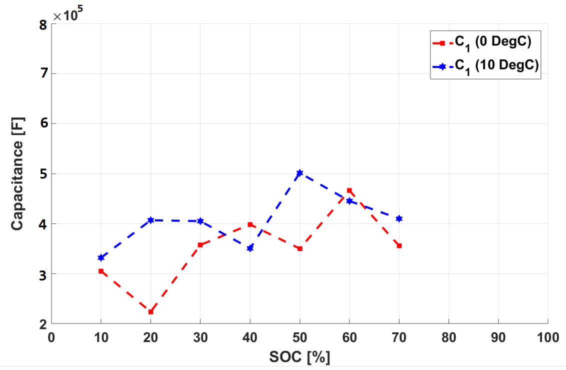

Figure 8.8: AutoLion C_1

The capacitance C_2 parameters from the experiment and the simulation method presents the fluctuating trend and showing the rise in capacitance with rise in temperature, as shown in fig 8.9 and 8.10. The difference in the respective parameter represents their different time constants. As, time constants from experimental test are shown in the results where as the time constants from the GT-Suite-AutoLion was not identified due to software limitations.

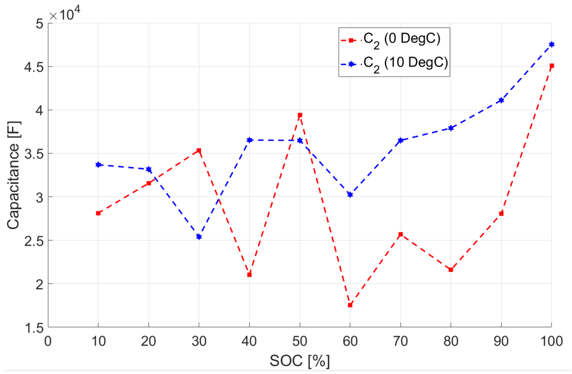

Figure 8.9: Experimental C_2

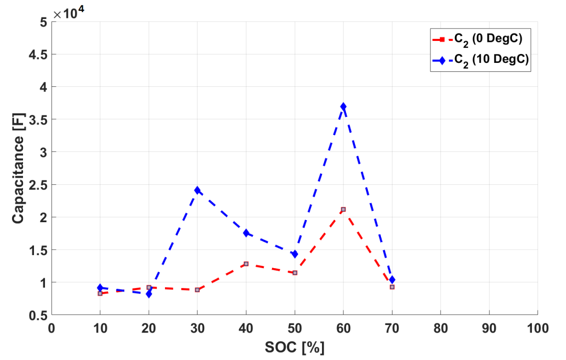

Figure 8.10: AutoLion C_2

Conclusively, the AutoLion parameters are identified till 70% SoC level which shows that the electrochemical model cell reached its upper cut off voltage limit sooner than expected, which might be due to few parameters in the designed model have higher or lower default values which affect the model cells' performance indeliberately. secondly, the modeled cell was reaching its upper limit due to the higher current that is 2C-rate. Therefore, there is scope research for cell balancing with necessary parameters and optimizing the modeled cell to identify the approximate value of the various parameters.

Besides estimating and comparing parameters, the comparison between OCV profiles from the experimental and the simulation data set was also presented in the given fig 8.11 and 8.12, which shows that the OCV profiles are similar for both experimental and simulation-based results. A slight rise in 10(°C) OCV profile can be observed for both experimental as well as simulation-based voltage profile but the simulated parameter have suggested that the electrochemical model reaches to its upper cutoff voltage limits sooner than expected.

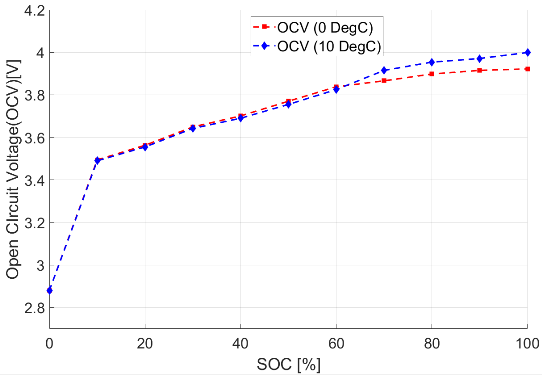

Figure 8.11: Experimental OCV profile

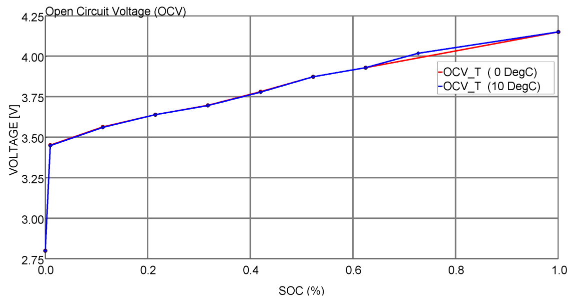

Figure 8.12: Simulated OCV profile

8.2 GTSuite-AutoLion Optimization model results

Although, the first optimization of the modeled cell was performed to determine the initial anticipated error, subsequently, other estimated parameters were added to balance the modelled cell, which improved the optimized results. And, these are differentiated in respected cases as presented in the given table 8.1.

Table 8.1: Various parameters for optimization of the modelled cell

Cases	Description
Case A	Default Parameters for Optimization
Case B	Case A + increased contact resistance
Case C	Case A + reduced contact resistance and particle size
Case D	Case C + diffusivity and electrolyte conductivity

A charging profile is chosen to calibrate as $2RC$ parameters were calculated on the basis of the charging profile from the experimental test and from the AutoLion model cell. After implementing the parameters mentioned in table 7.1 in the optimization model, the optimization model tried to match the AutoLion result with the experimental result. Fig 8.13 represents the optimized result with default parameters, however, for this optimization result, the initial N/P ratio was chosen as 1.35. And, parameters such as exchange current density and entropic heat for the electrodes whereas ionic conductivity and diffusivity parameters were neglected for the electrolyte.

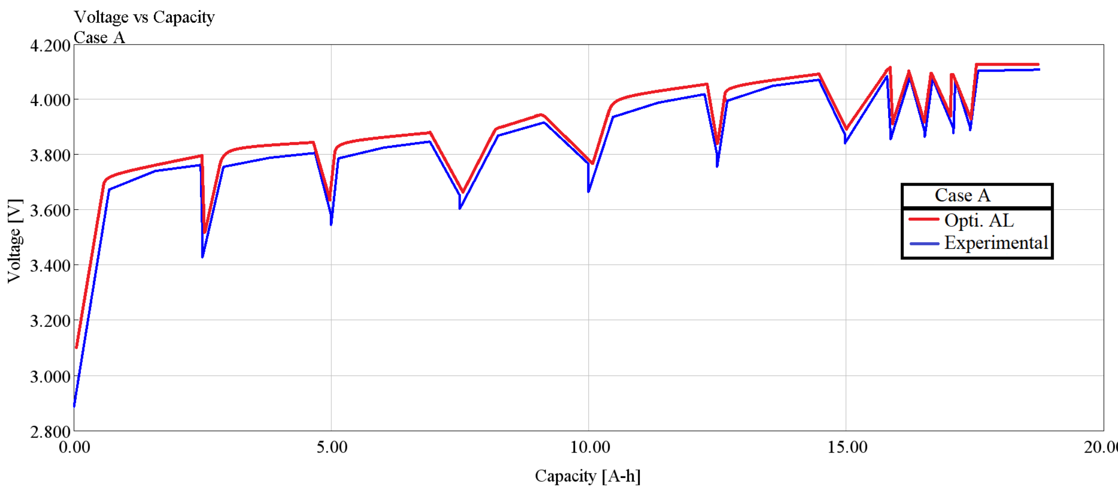

Figure 8.13: Optimization result between experimental and GTSuite simulation results

In fig 8.13, the result obtained after implementing the default parameters from table 7.1 in the optimization model, which shows the error of more than 3% in the optimized results. This result shows a constant difference in the OCV between the experimental and the optimized AutoLion results. This is due to a difference in the ohmic resistance of the battery cell. In the battery cell, there are various sources of ohmic resistance, such as resistivity of current collectors, the resistivity of electrodes and the contact resistance between the electrodes and electrolyte. The contact resistance between the electrodes and the current collectors is the important parameter to consider to tune the resistivity in the modeled cell as discussed earlier.

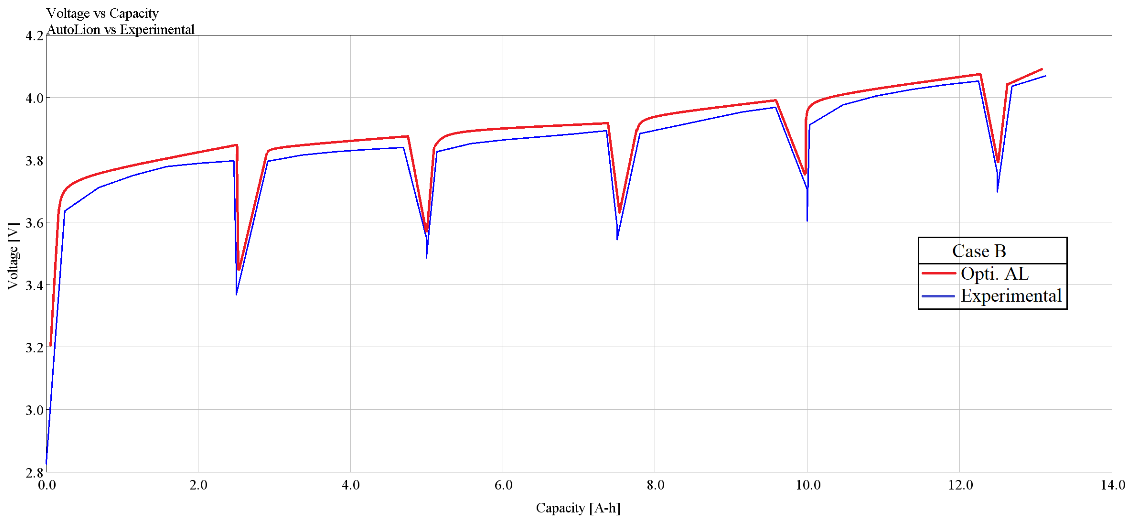

Figure 8.14: Optimized AutoLion simulation results for Case B

After updating the contact resistance parameter from the default value to the estimated value, a similar optimized result was obtained with the increased contact resistance, which shows that the upper cutoff voltage reached sooner and thus reducing the useful capacity of the battery cell, which is shown in fig 8.14. But, after reducing the contact resistance and reducing particle size, the previous curve got updated presenting the increase in useful capacity, shown in fig 8.15. So, the contact resistances play a role in determining the useful capacity of the battery cell.

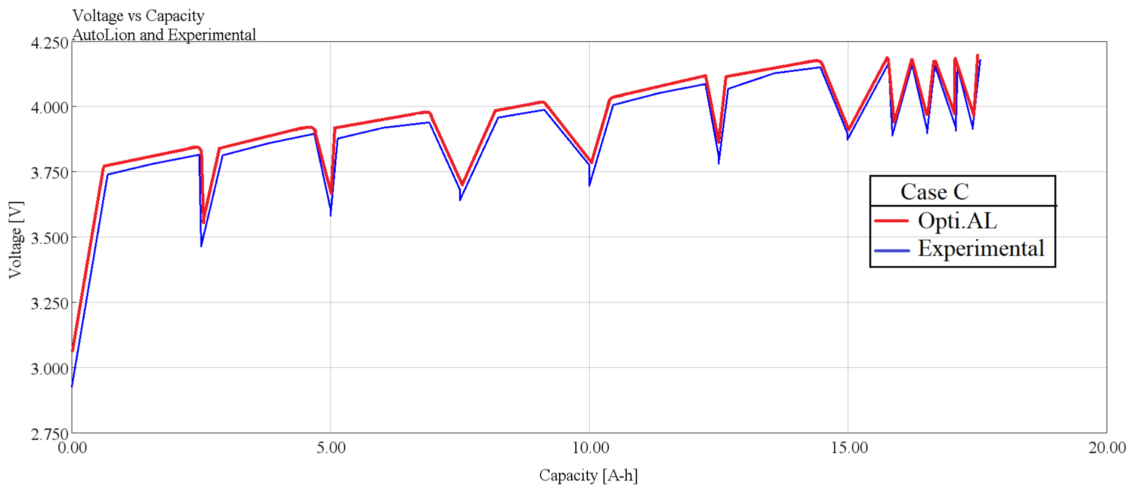

Figure 8.15: Optimized AutoLion results for Case C

The capacity of the AutoLion cell decreases with increasing C-rate, as the cell is charging with a $2C$-rate i.e 50A. This behavior is due to a deficiency of transport of

Li^+ ions when compared with the experimental cell. As, for all previous simulations, the diffusivity, conductivity of ions for the electrode and the electrolyte are assumed to be default values, but for next simulation, the parameters for the electrode and the electrolyte given in table 2.2 and table 2.3 were considered for the optimization of the battery cell. The reduced particle size and contact resistance have increased the useful capacity of the battery cell but the inclusion of diffusivity for the electrode and ionic diffusivity and ionic conductivity for the electrolyte, leads to a further increase in useful capacity of the battery cell, which is shown in fig 8.16. The N/P ratio helps to get a more optimized AutoLion OCV curve with the experimental OCV curve, which was used to balance the modeled cell as explained earlier.

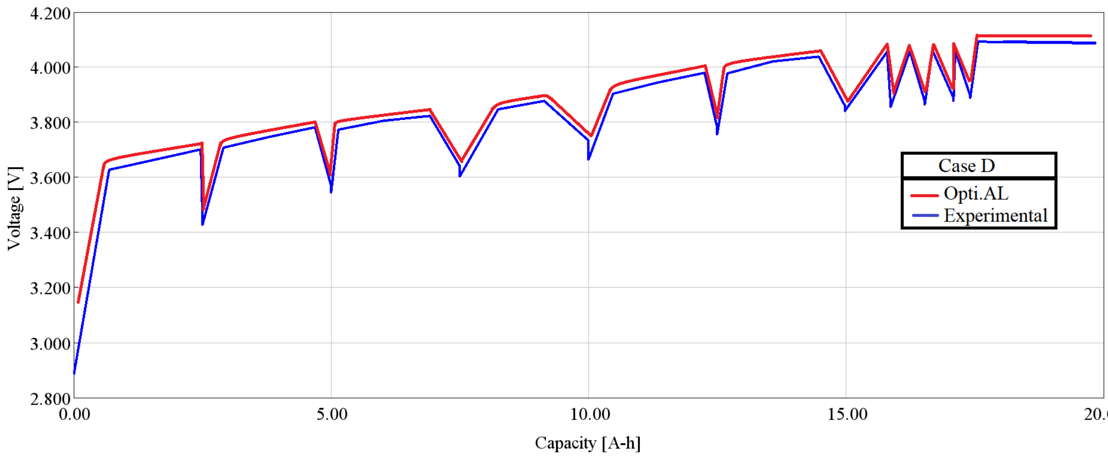

Figure 8.16: Optimized result with additional parameters

Although, the optimized AutoLion OCV curve is closed to the experimental result and the error of the optimized result was reduced to 2% but couldn't approach the expected result of 1%, which can be achieved by balancing the modelled cell with accurate parameters and these parameters can be found by doing research about the relevant parameters.

8.3 Calendar Aging effect on battery cell

Calendar aging might degrade the battery cell's capacity over a bench length. The calendar aging process of the battery cell is a slow degradation process at room temperature and retain most of its capacity, independent of its charged capacity but if the battery cell kept under higher or lower temperature, this can increase the degradation of the battery cell which can decrease the battery cell's useful capacity, as mentioned by [9]. Therefore, there wouldn't be much difference in the performance of the newly manufactured battery cell and the cell with a bench length of almost 2 years, which can be validated by comparing their ECM parameters.

9
Conclusion

A battery cooling system was designed incorporating a PID control system and tested with two different physical setups, the dummy cell, and the battery cell. The respective PID controller parameters were estimated by using basic tuning rules and implemented by using a python algorithm. A peristaltic pump with an inbuilt flow meter, an ice- chiller, two different temperature sensors with two different Arduino micro controller are integrated in the system to control the flow rate of the coolant and to maintain the surface temperature of the battery cell to the desired value. A designed cooling aluminum plate was chosen and water was chosen as a coolant in the cooling system. The designed cooling system manages to maintain the temperature of the battery cell close to the reference temperature.

Matlab/Simulink models were developed and the battery cell cooling system was considered as an electro-thermal model and the thermal parameters are found by inspecting measured step response. Additionally, the specific heat of the battery cell was also measured, which was found 1.15 $J/(g.K)$.

By performing a Hybrid power pulse characterization (HPPC) test for a charging-discharging cycle of the battery cell, the charging OCV waveform was selected to estimate the RC parameters, which varied with ambient temperature and at each SOC level. These RC parameters were compared to a model of an electrochemical battery cell in GT-Suite-AutoLion. Key battery parameters were identified and their individual influence on the modeled battery cell performance were discussed and presented with the optimized results. The optimized results for the OCV profile were not as good because the error in the results is more than 3% with default parameters, which reduced by 1% after adding the identified battery cell parameters and calibrating the modeled cell. However, the parameters which play a role in affecting the battery cell performance such as, ionic conductivity, diffusivity and degradation parameters such as SEI layer formation would be useful to analyze more in order to improve the accuracy of the GTSuite AutoLion. Lastly, the battery thermal management model can also be developed using the GT-Suite AutoLion to identify the heat generation and distribution inside the battery cell which can help in developing a cooling mechanism for the battery cell or the battery pack in GT-Suite-AutoLion.

Bibliography

[1] Yonghuang Ye, Lip Huat Saw, Yixiang Shi, Karthik Somasundaram, and Andrew A.O. Tay. Effect of thermal contact resistances on fast charging of large format lithium ion batteries. *Electrochimica Acta*, 134:327–337, 2014.

[2] Liqiang Zhang, Chao Lyu, Gareth Hinds, Lixin Wang, Weilin Luo, Jun Zheng, and Kehua Ma. Parameter Sensitivity Analysis of Cylindrical LiFePO 4 Battery Performance Using Multi-Physics Modeling. *Journal of The Electrochemical Society*, 161(5):A762–A776, 2014.

[3] Qian Sun and Chengjun Tang. Battery cell electro-thermal modeling and cooling system design. 2018.

[4] Akihiko Maruyama. Automotive Lithium-ion Batteries. pages 330–334.

[5] Awais Chaudhry. Investigation of Lithium-ion battery parameters using pulses and EIS. 2017.

[6] Stefan Skoog. Parameterization of equivalent circuit models for high power lithium-ion batteries in HEV applications. *2016 18th European Conference on Power Electronics and Applications, EPE 2016 ECCE Europe*, pages 1–10, 2016.

[7] Ali Jokar, Barzin Rajabloo, Martin Désilets, and Marcel Lacroix. Review of simplified Pseudo-two-Dimensional models of lithium-ion batteries. *Journal of Power Sources*, 327(September):44–55, 2016.

[8] Shovon Goutam, Jean-marc Timmermans, Noshin Omar, Peter Van Den Bossche, Joeri Van Mierlo, Lide Rodriguez, Nerea Nieto, and Maciej Swierczynski. Surface temperature evolution and the location of maximum and average surface temperature of a lithium-ion pouch cell under variable load profiles . (December):1–7, 2014.

[9] Evelina Wikner. Lithium ion Battery Aging : Battery Lifetime Testing and Physics-based Modeling for Electric Vehicle Applications. 2017.

[10] Robyn Jackey, Michael Saginaw, Pravesh Sanghvi, Javier Gazzarri, Tarun Huria, and Massimo Ceraolo. Battery Model Parameter Estimation Using a Layered Technique: An Example Using a Lithium Iron Phosphate Cell. *SAE Technical Paper Series*, 1(April), 2013.

[11] U Iraola, I Aizpuru, J M Canales, A Etxeberria, and I Gil. Methodology for thermal modelling of lithium- ion batteries. pages 6752–6757, 2013.

[12] D Bernardi, E Pawlikowski, and J Newman. A General Energy Balance for Battery Systems. 132(1), 1970.

[13] Stefan Skoog. Electro-thermal modeling of high-performance lithium-ion energy storage systems including reversible entropy heat. *Conference Proceedings -*

IEEE Applied Power Electronics Conference and Exposition - APEC, pages 2369–2373, 2017.

[14] Ahmad A Pesaran and Matthew Keyser. Thermal Characteristics of Selected EV and HEV Batteries. 2001.

[15] Wei Lai and Francesco Ciucci. Electrochimica Acta Mathematical modeling of porous battery electrodes — Revisit of Newman ' s model. *Electrochimica Acta*, 56(11):4369–4377, 2011.

[16] Johannes Kasnatscheew, Tobias Placke, Benjamin Streipert, Sergej Rothermel, Ralf Wagner, Paul Meister, Isidora Cekic Laskovic, and Martin Winter. A Tutorial into Practical Capacity and Mass Balancing of Lithium Ion Batteries. *Journal of The Electrochemical Society*, 164(12):A2479–A2486, 2017.

[17] Cheon Soo Kim, Kyung Min Jeong, Keon Kim, and Cheol Woo Yi. Effects of capacity ratios between anode and cathode on electrochemical properties for lithium polymer batteries. *Electrochimica Acta*, 155:431–436, 2015.

[18] Joongpyo Shim and Kathryn A Striebel. Characterization of High-Power Lithium-Ion Cells During Constant Current Cycling Part I . Cycle Performance and Electrochemical Diagnostics. pages 1–24.

[19] Sara Taslimi Taleghani, Bernard Marcos, Karim Zaghib, and Gaétan Lantagne. A Study on the Effect of Porosity and Particles Size Distribution on Li-Ion Battery Performance. *Journal of The Electrochemical Society*, 164(11):E3179–E3189, 2017.

[20] Ali Dareini. Prediction and analysis of model's parameters of Li-ion battery cells. 2016.

[21] Dinesh Bista. Understanding and Design of an Arduino-based PID Controller Understanding and Design of an Arduino- based PID Controller. 2016.

[22] E. Cheres. Parameter estimation of an unstable system with a PID controller in a closed loop configuration. *Journal of the Franklin Institute*, 343(2):204–209, 2006.

[23] Radek Matušů. Calculation of all stabilizing PI and PID controllers. *International Journal of Mathematics and Computers in Simulation*, 5(3):224–231, 2011.

[24] Sigurd Skogestad. Probably the best simple PID tuning rules in the world. 2001.

[25] Subhransu Padhee. Controller design for temperature control of heat exchanger system: Simulation studies. *WSEAS Transactions on Systems and Control*, 9(1):485–491, 2014.

[26] Shahabeddin K Mohammadian, Ya-ling He, and Yuwen Zhang. Internal cooling of a lithium-ion battery using electrolyte as coolant through microchannels embedded inside the electrodes. *Journal of Power Sources*, 293:458–466, 2015.

[27] Satyam Panchal, Scott Mathewson, Roydon Fraser, Richard Culham, and Michael Fowler. Thermal Management of Lithium-Ion Pouch Cell with Indirect Liquid Cooling using Dual Cold Plates Approach. *SAE International Journal of Alternative Powertrains*, 4(2):293–307, 2015.

[28] Cristina Pitorac. Estimation of the Power Losses of a Li-Ion Battery by Operation in an Electric Vehicle. 2016.

[29] Sandeep Nital David. Pulse power characterisation for lithium ion cells in automotive applications Small and large signal cell impedance analysis. 2016.

A

Appendix 1

I) Power-Flow rate Matlab code

```
    %% Calculations for waterflow
clear all; close all; clc;
%Cp = 4.186; % [J/g*K], constant
Cp = 4.288298;
%Rho = 997; % [g/l], constant
Rho = 995;
T_delta = 2.2; %[K], input
P_loss = 2:10:100; % Assumed power loss in [W], input
%P_loss = 100;

V_dot = P_loss / (Cp*Rho*T_delta) * 60 % Waterflow in [l/min]


plot(P_loss,V_dot*1000)
xlabel('Power loss(Watts)')
ylabel('flow rate per minute(mL/min)')
grid on

%% Calculations for power of known waterflow and temp. diff.
clear all; close all; clc;
Cp = 4.186; % [J/g*K], constant
Rho = 997; % [g/l], constant
T_delta = 0.03; %Measured temp. diff. in [K], input
V_dot = 0.13; % Measured waterflow in [l/min], input

P_loss = Cp*Rho*T_delta*V_dot/60 % Power loss in [W]

%% Calculations for deltaT of known waterflow and Power loss.
clear all; close all; clc;
Cp = 4.186; % [J/g*K], constant
Rho = 997; % [g/l], constant
V_dot = 0.05; % Measured waterflow in [l/min], input
P_loss = 0:10:50; % [W], input

T_delta = P_loss * 60 / (Cp*Rho*V_dot) % Temp diff in [K] or [degC]
plot(P_loss,T_delta,'g','LineWidth',3)
```

```
hold on
V_dot = 0.1;
T_delta = P_loss * 60 / (Cp*Rho*V_dot) % Temp diff in [K] or [degC]
V_dot = 0.2;
plot(P_loss,T_delta,'r','LineWidth',3)
hold on
T_delta = P_loss * 60 / (Cp*Rho*V_dot) % Temp diff in [K] or [degC]
plot(P_loss,T_delta,'b','LineWidth',3)
hold on
set(gca,'FontSize',24)
set(gca,'ytick',0:2.5:17.5)
title('Impact of flowspeed on Temperature Difference')
legend('50 ml/min','100 ml/min','200 ml/min')
xlabel('Input Power, [W]')
ylabel('Difference in Temperature, [K]')
grid on
%% Calculations for conversion from ml/min to m/s for certain tube size
clear all; close all; clc;
%m/s = (l/min) * (m^3/l) / (m^2) (1/60 min/s)
% 1/1000 (m^3/l)
V_dot = 0.0588; % Measured waterflow in [l/min], input
radius = 0.004; % [m], input
v = V_dot  / ((pi*radius^2) * 60 *1000)

v = 0.0165
V_dot = v *((pi*radius^2) * 60 *1000)
```

II) **PID control Arduino code**

```
/*    Max6675 Module  ==>   Arduino
 *    CS              ==>     D10
 *    SO              ==>     D12
 *    SCK             ==>     D13
 *    Vcc             ==>     Vcc (5v)
 *    Gnd             ==>     Gnd      */

#include <Wire.h>
#include <LiquidCrystal_I2C.h>

/*    i2c LCD Module  ==>   Arduino
 *    SCL             ==>     A5
 *    SDA             ==>     A4
 *    Vcc             ==>     Vcc (5v)
 *    Gnd             ==>     Gnd      */

#include <SPI.h>
//We define the SPI pìns
#define MAX6675_CS   10
```

```
#define MAX6675_SO   12
#define MAX6675_SCK  13

#define MAX6675_CS1   5
#define MAX6675_SO1   7
#define MAX6675_SCK1  8

//Pins
int PWM_pin = 3;

//Variables
float temperature_read = 0.0;
float set_temperature = 20;
float PID_error = 0;
float previous_error = 0;
float elapsedTime, Time, timePrev;
int PID_value = 0;
int PID_main = 0;

//PID constants
int kp = 5;   int ki = 15.03 ;   int kd = 2.5;
int PID_p = 0;    int PID_i = 0;    int PID_d = 0;

void setup() {
  pinMode(PWM_pin,OUTPUT);
  TCCR2B = TCCR2B & B11111000 | 0x03;
  // pin 3 and 11 PWM frequency of 980.39 Hz
  Time = millis();
  lcd.begin(16,2);
  lcd.backlight();
Serial.begin(9600);
}

void loop() {

  float temperature_read_1 = readThermocouple_1();

 // First we read the real value of temperature
  temperature_read = readThermocouple();
  //Next we calculate the error between the setpoint and the real value
  PID_error = set_temperature - temperature_read;
  //Calculate the P value
  PID_p = kp * PID_error;
  //Calculate the I value in a range on +-3
  if(-3 < PID_error <3)
  {
```

```
    PID_i = PID_i + (ki * PID_error);
  }
  //For derivative we need real time to calculate speed change rate
  timePrev = Time;   // the previous time is stored before the actual time read
  Time = millis();  // actual time read
  elapsedTime = (Time - timePrev) / 1000;
  //Now we can calculate the D calue
  PID_d = kd*((PID_error - previous_error)/elapsedTime);
  //Final total PID value is the sum of P + I + D
  PID_value = PID_p + PID_i + PID_d;
  PID_main= PID_value * 3.8;
  //We define PWM range between 0 and 255
  if(PID_main < 0)
  {    PID_main = 0;    }
  if(PID_main > 255)
  {    PID_main = 255;  }

//Now we can write the PWM signal to the mosfet on digital pin D3
(PWM_pin,255-PID_value)

//PID_main= PID_value * 10;
  analogWrite(PWM_pin,255-PID_main);
  previous_error = PID_error;

//Remember to store the previous error for next loop.

Serial.print(temperature_read_1);
Serial.print(" ");
Serial.print(temperature_read);
Serial.println();
 delay(300);
  lcd.clear();

  lcd.setCursor(0,0);
  lcd.print("PID Model");
  lcd.setCursor(10,0);
  lcd.print("R:");
   lcd.setCursor(12,0);
  lcd.print(temperature_read_1,0);
  lcd.setCursor(0,1);
  lcd.print("S:");
  lcd.setCursor(2,1);
  lcd.print(set_temperature,1);
  lcd.setCursor(10,1);
  lcd.print("R:");
  lcd.setCursor(12,1);
```

```
  lcd.print(temperature_read,1);
}

double readThermocouple() {

  uint16_t v;
  pinMode(MAX6675_CS, OUTPUT);
  pinMode(MAX6675_SO, INPUT);
  pinMode(MAX6675_SCK, OUTPUT);

  digitalWrite(MAX6675_CS, LOW);
  delay(1);

  // Read in 16 bits,
  //  15    = 0 always
  //  14..2 = 0.25 degree counts MSB First
  //  2     = 1 if thermocouple is open circuit
  //  1..0  = uninteresting status

  v = shiftIn(MAX6675_SO, MAX6675_SCK, MSBFIRST);
  v <<= 8;
  v |= shiftIn(MAX6675_SO, MAX6675_SCK, MSBFIRST);

  digitalWrite(MAX6675_CS, HIGH);
  if (v & 0x4)
  {
    // Bit 2 indicates if the thermocouple is disconnected
    return NAN;
  }

  // The lower three bits (0,1,2) are discarded status bits
  v >>= 3;

  // The remaining bits are the number of 0.25 degree (C) counts
  return v*0.25;
}

double readThermocouple_1()
 {

  uint16_t v1;
  pinMode(MAX6675_CS1, OUTPUT);
  pinMode(MAX6675_SO1, INPUT);
  pinMode(MAX6675_SCK1, OUTPUT);

  digitalWrite(MAX6675_CS1, LOW);
```

```
  delay(1);

  // Read in 16 bits,
  //  15    = 0 always
  //  14..2 = 0.25 degree counts MSB First
  //  2     = 1 if thermocouple is open circuit
  //  1..0  = uninteresting status

  v1 = shiftIn(MAX6675_SO1, MAX6675_SCK1, MSBFIRST);
  v1 <<= 8;
  v1 |= shiftIn(MAX6675_SO1, MAX6675_SCK1, MSBFIRST);

  digitalWrite(MAX6675_CS1, HIGH);
  if (v1 & 0x4)
  {
    // Bit 2 indicates if the thermocouple is disconnected
    return NAN;
  }

  // The lower three bits (0,1,2) are discarded status bits
  v1 >>= 3;

  // The remaining bits are the number of 0.25 degree (C) counts
  return v1*0.25;
}
```

III) Algorithm to estimate PID parameters

```
import numpy as np
%matplotlib inline
import matplotlib.pyplot as plt
from scipy.integrate import odeint
import ipywidgets as wg
from IPython.display import display
n = 2500 # time points to plot
tf = 400.0 # final time
SP_start = 25  # time of set point change

def process(y,t,u):
    Kp = 5.0
    taup = 2.0
    thetap = 1.0
    if t<(thetap+SP_start):
        dydt = 0.0  # time delay
    else:
        dydt = (1.0/taup) * (-y + Kp * u)
    return dydt
```

```
def pidPlot(Kc,tauI,tauD):
    t = np.linspace(0,tf,n)
    P= np.zeros(n)
    I = np.zeros(n)
    D = np.zeros(n)
    e = np.zeros(n)
    OP = np.zeros(n)
    PV = np.zeros(n)
    SP = np.zeros(n)
    SP_step = int(SP_start/(tf/(n-1))+1) # setpoint start
    SP[0:SP_step] = 0.0
    SP[SP_step:n] = 27.0
    y0 = 0.0
    # loop through all time steps
    for i in range(1,n):
        # simulate process for one time step
        ts = [t[i-1],t[i]]
        y = odeint(process,y0,ts,args=(OP[i-1],))  # compute next step
        y0 = y[1]
        # calculate new OP with PID
        PV[i] = y[1]
        e[i] = SP[i] - PV[i]
        dt = t[i] - t[i-1]
        P[i] = Kc * e[i]
        I[i] = I[i-1] + (Kc/tauI) * e[i] * dt  # calculate integral term
        D[i] = -Kc * tauD * (PV[i]-PV[i-1])/dt # calculate derivative term
        OP[i] = P[i] + I[i] + D[i] # calculate new controller output

    # plot PID response
    plt.figure(1,figsize=(50,25))
    plt.plot(t,SP,'k-',linewidth=4,label='Setpoint (SP)')
    plt.plot(t,PV,'r:',linewidth=4,label='Process Variable (PV)')
    plt.legend(loc='best')

Kc_slide = wg.FloatSlider(value=0.1,min=-0.2,max=1.0,step=0.05)
tauI_slide = wg.FloatSlider(value=4.0,min=0.01,max=5.0,step=0.1)
tauD_slide = wg.FloatSlider(value=0.0,min=0.0,max=1.0,step=0.1)
wg.interact(pidPlot, Kc=Kc_slide, tauI=tauI_slide, tauD=tauD_slide)
```